UNIVERSIDADE ESTADUAL DE CAMPINAS
Faculdade de Engenharia Mecânica

DANILO ALCANTARA DE OLIVEIRA

Back Glass Contamination Numerical and Experimental Study of Automotive Vehicles

Estudo Numérico e Experimental da Contaminação dos Vidros Traseiros de Veículos Automotivos

CAMPINAS
2020

DANILO ALCANTARA DE OLIVEIRA

Back Glass Contamination Numerical and Experimental Study of Automotive Vehicles

Estudo Numérico e Experimental da Contaminação dos Vidros Traseiros de Veículos Automotivos

Dissertation presented to the School of Mechanical Engineering of the University of Campinas in partial fulfillment of the requirements for the degree of Master in Mechanical Engineering, in the area of Energy.

Dissertação apresentada à Faculdade de Engenharia Mecânica da Universidade Estadual de Campinas como parte dos requisitos exigidos para a obtenção do título de Mestre em Engenharia Mecânica, na Área de Energia. .

Orientador: Prof. Dr. Rogério Gonçalves dos Santos

ESTE TRABALHO CORRESPONDE À VERSÃO FINAL DA DISSERTAÇÃO DEFENDIDA PELO ALUNO DANILO ALCANTARA DE OLIVEIRA, E ORIENTADA PELO PROF. DR. ROGÉRIO GONÇALVES DOS SANTOS.

CAMPINAS
2020

Ficha catalográfica
Universidade Estadual de Campinas
Biblioteca da Área de Engenharia e Arquitetura
Rose Meire da Silva - CRB 8/5974

OL4b

Oliveira, Danilo Alcantara de, 1985-
Back glass contamination numerical and experimental study of automotive vehicles / Danilo Alcantara de Oliveira. – Campinas, SP : [s.n.], 2020.

Orientador: Rogério Gonçalves dos Santos.
Dissertação (mestrado) – Universidade Estadual de Campinas, Faculdade de Engenharia Mecânica.

1. Vidro - Estrutura. 2. Vidro - Tecnologia. 3. Lattice Boltzmann, Métodos de. 4. Fluidodinâmica computacional. 5. Túneis aerodinâmica. 6. Veículos a motor - Aerodinâmica. I. Santos, Rogério Gonçalves dos, 1978-. II. Universidade Estadual de Campinas. Faculdade de Engenharia Mecânica. III. Título.

Informações para Biblioteca Digital

Título em outro idioma: Estudo numérico e experimental da contaminação dos vidros traseiros de veículos automotivos
Palavras-chave em inglês:
Glass - Structure
Glass - Technology
Lattice Boltzmann, Methods
Computational fluid dynamics
Aerodynamic wind tunnel
Internal combustion engine vehicles - Aerodynamics
Área de concentração: Térmica e Fluídos
Titulação: Mestre em Engenharia Mecânica
Banca examinadora:
Rogério Gonçalves dos Santos [Orientador]
William Roberto Wolf
Dirceu Noriler
Data de defesa: 25-06-2020
Programa de Pós-Graduação: Engenharia Mecânica

Identificação e informações acadêmicas do(a) aluno(a)
- ORCID do autor: https://orcid.org/0000-0003-3526-8456
- Currículo Lattes do autor: http://lattes.cnpq.br/.

UNIVERSIDADE ESTADUAL DE CAMPINAS
FACULDADE DE ENGENHARIA MECÂNICA

DISSERTAÇÃO DE MESTRADO ACADÊMICO

Back Glass Contamination Numerical and Experimental Study of Automotive Vehicles

Estudo Numérico e Experimental da Contaminação dos Vidros Traseiros de Veículos Automotivos

Autor: Danilo Alcantara de Oliveira

Orientador: Prof. Dr. Rogério Gonçalves dos Santos

A Banca Examinadora composta pelos membros abaixo aprovou esta Dissertação:

Prof. Dr. Rogério Gonçalves dos Santos, Presidente
DE / FEM / UNICAMP

Prof. Dr. William Roberto Wolf
DE / FEM / UNICAMP

Prof. Dr. Dirceu Noriler
DEPro / FEQ / UNICAMP

A Ata de Defesa com as respectivas assinaturas dos membros encontra-se no SIGA/Sistema de Fluxo de Dissertação/Tese e na Secretaria do Programa da Unidade.

Campinas, 25 de agosto de 2020.

Dedicatória

Primeiramente a Deus e várias pessoas que me incentivaram a concluir esse trabalho: pais, irmãos e esposa.

Agradecimentos

General Motors no Brasil (Roberto Ramos, Eduardo Almeida, Gilvan Rossi) e General Motors nos EUA (Gena Vitale, Silvia Karlson, Marcelo Bertochi, Jacques Ndione, Ken Karbon, Donnell Johnson, Fernando Saito, David Caples, Flavio Sales) pelo incentivo de recursos e ajuda técnica para realizar esse trabalho; Daussalt Systems (Michael, Jonathan) pela ajuda técnica com o software, Rogerio Gonçalves dos Santos pela orientação, Mateus Marques pela ajuda de comunicação com a FEM e Flavio Sales e Jeovana Oliveira pelo incentivo.

Resumo

Nesse trabalho, uma definição e revisão sobre contaminação na superfície de veículos é apresentada, mostrando sua importância na segurança, visibilidade e satisfação visual do motorista. Esse estudo é focado em contaminação no vidro traseiro de veículos automotivos. Resultados de simulação numérica de um veículo real utilizando a técnica de Lattice-Boltzmann são validadas através de resultados experimentais obtidos em túnel de vento com veículo em escala real. O programa comercial PowerFLOW da empresa Daussault Systems é utilizado nas simulações numéricas e correlação com o teste físico. A simulação consiste em uma análise transiente, multifásica, tridimensional na qual se obtém resultados aerodinâmicos e de acúmulo de contaminantes na superfície do veículo. Alguns parâmetros geométricos tais como presença de spoiler no teto e variação do ângulo de inclinação do vidro traseiro foram estudados na simulação numérica. Alguns parâmetros não geométricos também foram investigados nesse estudo, tais como a taxa de vazão de contaminantes, velocidade do veículo e resolução da malha no modelo computacional. Os resultados do teste de túnel de vento e da simulação numérica foram bastante próximos e coerentes, permitindo validar a mesma. Isto evidencia que simulações numéricas podem ser utilizadas para tomadas de decisão, como por exemplo, na remoção do limpador do vidro traseiro. Uma nova metodologia foi utilizada para comparar os resultados de contaminação do vidro traseiro, que pode ser estendida para outras áreas no veículo. Tal metodologia consiste no índice de contaminação no qual o número de partículas é medido em uma determinada área para se efetuar uma comparação quantitativa dos resultados.

Palavras Chave: contaminação, vidro traseiro, CFD, Lattice-Boltzmann, túnel de vento.

Abstract

A review and definition of contamination on vehicle surface is presented herein, showing its importance on safety, vision and visual satisfaction of the driver. This study is focused on automobile vehicle back glass contamination. Numerical simulation results of a real vehicle using Lattice-Boltzmann are validated in a full-scale wind tunnel experimental test. The commercial software PowerFLOW by Daussault System is used to perform the numerical simulations and correlation with physical tests. The simulation consists in a transient, multiphase and tridimensional analysis, where aerodynamics and contamination build-up are measured on the vehicle surface. Some geometric parameters such as the presence of roof spoiler and back light angle inclination were studied using the numerical simulation. Some non- geometric parameters were also investigated in this study, such as contaminants flow rate, vehicle speed and mesh resolution in the computational model. The wind tunnel test results and the numerical simulation results were very similar and comparable, allowing the software validation. That highlights that numerical simulations can be used to take decisions, for instance, the rear wiper removal. A new technology was used to compare the back glass contamination results, which can be extended to other areas on the vehicle. Such methodology consists in the contamination index, where the number of particles are counted on a determined area to compare the results qualitatively.

Key Word: contamination, back glass, CFD, Lattice-Boltzmann, wind tunnel.

Sumário

1 OBJETIVO

O objetivo geral deste trabalho foi utilizar ferramentas numéricas de CFD para estudar contaminação no vidro traseiro de veículos automotivos. Dessa forma, é possível determinar se alguns artifícios, tais como limpador do vidro traseiro, são necessários ou não para manter o vidro traseiro limpo de contaminantes e assegurar a visão do motorista. Essa informação é importante para tomadas de decisão no início de projetos, afim de se estimar o custo de peças e massa do veículo, bem como em desenvolver o formato do teto e ângulo do vidro traseiro visando em baixa contaminação. Para isso, três estudos separados foram realizados em diferentes artigos.

O objetivo do primeiro artigo, com o título "*VEHICLE REAR END CONTAMINATION COMPARISON USING NUMERICAL SIMULATION AND WIND TUNNEL TEST*", foi validar a ferramenta de simulação numérica. Portanto, um teste em escala real no túnel de vento climático da General Motors localizado em Warren, MI - EUA foi feito pelo autor do artigo juntamente com os técnicos do laboratório e outros engenheiros de teste. Nesse experimento, foram realizados testes de chuva e de auto-contaminação (quando carro passa por uma estrada suja) em um veículo comercial e posteriormente, comparados com as simulações de CFD.

Uma vez estabelecida a correlação entre o modelo de simulação numérica e o teste físico no túnel de vento, um próximo estudo foi feito. O objetivo do segundo artigo, com o título "*CASE STUDY OF VEHICLE BACK GLASS CONTAMINATION WITH AND WITHOUT SPOILER*" foi identificar qual é o caso crítico para visão do motorista pela vidro traseiro: auto-contaminação ou chuva. Dessa forma, é possível focar em apenas uma das simulações durante o desenvolvimento de novos projetos, reduzindo recursos computacionais e humanos.

Através da conclusão do segundo artigo, no qual identificou a auto-contaminação como sendo o caso crítico para visão do motorista pelo vidro traseiro, um terceiro estudo foi feito utilizando a condição de auto-contaminação. O objetivo do terceiro artigo, com o título "*STUDY OF THE REAR BACKLIGHT ANGLE INFLUENCE ON VEHICLE AERODYNAMICS AND CONTAMINATION*", foi validar a relação entre o ângulo de inclinação do vidro traseiro com o coeficiente de arrasto estudado por Hucho et al. (1976) e relacioná-los com a contaminação no vidro traseiro. Esse estudo possibilita desenvolver veículos com ângulo de inclinação favorável a um baixo coeficiente de arrasto e baixa contaminação no vidro traseiro, evitando a utilização de limpadores do vidro traseiro e reduzindo massa.

2 METODOLOGIA

2.1 METODOLOGIA EXPERIMENTAL

Os resultados experimentais foram utilizados no primeiro artigo cujo título é "*VEHICLE REAR END CONTAMINATION COMPARISON USING NUMERICAL SIMULATION AND WIND TUNNEL TEST*". Tais resultados foram utilizados para comparação e validação do modelo de simulação numérica.

O experimento consiste em testes realizados no túnel de vento climático em escala real da General Motors em Warren, MI – EUA. Os testes foram efetuados em 19 de Junho de 2019 pelo autor deste trabalho, por mais dois engenheiros do departamento de aerodinâmica e um técnico do laboratório. O teste foi realizado exclusivamente com os fins de comparação com os resultados da simulação para construir credibilidade na análise numérica no tocante a contaminação do vidro traseiro. Esse túnel de vento pode promover temperaturas de -40ºC até +60ºC, de 5% a 95% de umidade relativa e velocidades do vento de até 240km/h. Ele é equipado com sistema de dinamômetros que permitem as rodas dos carros testados girarem e a sessão de teste possui 13m de comprimento. Esse túnel é utilizado para estudar casos de contaminação por chuva no vidro lateral e retrovisor, e também para avaliar casos térmicos, tais como exposição ao sol, arrefecimento de motor e monitoramento de temperatura de componentes.

Para os testes de auto-contaminação e chuva, foram utilizados três bicos injetores conectados por um tubo como emissores do fluído. Os injetores são da marca *Lechler* modelo 502-548, espaçados 0.75m de distância entre eles, a bomba e reservatório de fluído são produzidos pela *Fimco*, modelo LG-25-HV (com uma vazão média de 7.2L/min) e o *timer relay* utilizado foi o modelo TD-71526 produzido pela *Macromatic*. Como fluido, uma mistura de água com um contraste em forma de pó D-282 (nome químico *C. I. Fluorescent Brightener 220*) produzido pela *DayGlo* em Ohio – EUA, foi utilizada para facilitar a visualização das partículas de água, na proporção 1% de contraste para cada 10% de volume de água. Tal mistura, quando submetida sob a luz ultravioleta, reluz e é facilmente identificável o caminho percorrido pelo fluido. A luz ultravioleta utilizada foi o modelo UV Panel HP 4x4 LL-UV P40, do fabricante *ADJ Products*. O veículo em escala real utilizado foi o Chevrolet Volt modelo 2015, o qual foi fixado no chão do túnel por meio de correntes de aço com guinchos nas áreas de reboque o carro e apenas as rodas traseiras estavam sobre o dinamômetro rotacionando.

Todas imagens de resultados de teste foram fotografadas com a câmera *Panasonic* DMC-FZ1000 com resolução 2736x1824.

Durante o teste, o túnel de vento era ligado até o fluxo de ar estabilizar na velocidade desejada. Para os casos estudados, foram rodados 50km/h e 100km/h. Uma vez estabilizada a velocidade, os injetores eram acionados, injetando o fluido no fluxo de ar por 80s. Após esse passo, o fluxo de ar era desligado e era possível entrar na sessão de testes para observar o fluxo de água e fotografar. Antes de efetuar uma próxima iteração, a superfície do carro era secada manualmente para garantir que o fluido do teste anterior não afetaria o resultado do teste seguinte. E esse procedimento era repetido para cada iteração de velocidade do ar ou posição dos bicos emissores. O tempo total de teste foi de 10 horas aproximadamente.

Algumas diferentes posições de emissores foram estudadas dependendo do tipo de teste desejado. Para o caso de chuva, os injetores da mistura de água e contraste foram posicionados na frente do modelo, direcionados na direção contrária do fluxo de ar, afim de promover uma distribuição homogênea da mistura sobre a superfície do carro. A altura dos emissores em relação ao chão do túnel também foi variada, partindo de 0.75m, 1.10m até 1.50m, para garantir que o fluido estava atingindo a região do vidro traseiro do veículo. A distância do parachoques do carro até os emissores foi de 1.50m.

Para os casos de auto-contaminação, o duto onde os injetores estão conectados não era longo o suficiente para cobrir a largura total do carro, portanto apenas o lado esquerdo do veículo foi avaliado. Os injetores foram posicionados primeiramente a frente da roda traseira esquerda, a 0.17m de distância do chão do túnel e 0.17m de distância da roda traseira. Uma segunda configuração também foi estudada para certificar de que a velocidade inicial da mistura emitida pelo injetor não afetaria o resultado. Nessa outra configuração, os injetores foram posicionados a 0.13m de distância do chão do túnel e 0.23m de distância da roda traseira esquerda. A escolha da posição dos injetores foi a mais próxima do pneu e do chão possível, mantendo a devida segurança dos equipamentos. Em todos os casos, da mesma forma que os casos de chuva, a velocidade do fluxo de ar no túnel foi de 50km/h e 100km/h.

Essa metodologia utilizada neste trabalho é considerada *estado da arte* com relação a testes de contaminação em túnel de vento climático por Shilling et al. (2020). Com respeito ao pós-processamento dos resultados, é possível fazer uma comparação visual e qualitativa entre as fotografias tiradas ao final de cada ensaio. Para obter-se também uma análise quantitativa, um programa no *Matlab* foi desenvolvido pela General Motors com a participação do autor desse trabalho. Tal programa consiste em contabilizar os pixels de uma imagem e, pela diferenciação das cores, calcular a porcentagem de fluido reluzente em uma determinada área.

Dessa forma, uma metodologia objetiva foi utilizada para comparar os resultados entre as fotos tiradas durante o teste no túnel de vento e também poderia ser utilizada para comparar com os resultados da simulação numérica.

2.2 METODOLOGIA NUMÉRICA

Modelos de simulação numérica foram utilizado nos três artigos apresentados nesse trabalho. No primeiro artigo, com o título "*VEHICLE REAR END CONTAMINATION COMPARISON USING NUMERICAL SIMULATION AND WIND TUNNEL TEST*", os modelos matemáticos dos veículos comerciais Chevrolet Volt modelo 2015 e Chevrolet Malibu Maxx modelo 2005 foram escolhidos para esse estudo e nos artigos seguintes, com os títulos "*CASE STUDY OF VEHICLE BACK GLASS CONTAMINATION WITH AND WITHOUT SPOILER*" e "*STUDY OF THE REAR BACKLIGHT ANGLE INFLUENCE ON VEHICLE AERODYNAMICS AND CONTAMINATION*", respectivamente, apenas o modelo matemático do Chevrolet Malibu Maxx foi utilizado.

Os modelos matemáticos originais, obtidos do banco de dados da General Motors, possuem todos os componentes e detalhes geométricos de um carro real de produção. Contudo, algumas simplificações foram feitas para se realizar as simulações numéricas em CFD. No caso do Chevrolet Volt, os detalhes de *gaps* entres os painéis externos foram removidos, de forma que a cabine se tornou um único volume selado, isto é, sem aberturas que permita com que haja fluxo de ar entre o interior da cabine e o ambiente externo. Outras simplificações, tais como remover as ranhuras dos pneus e a remoção da espessura dos componentes (considerando apenas a superfície exterior) também diferem do modelo matemático original. No modelo do Malibu Maxx, além das simplificações já mencionadas acima, a abertura da entrada de ar para o motor no parachoques do veículo foi bloqueada e o assoalho do carro simplificado de maneira em que se tornasse uma placa plana. Todas essas alterações foram efetuadas a fim de reduzir o custo computacional das simulações numéricas.

Uma vez que a geometria do modelo computacional foi ajustada, inicia-se o processo de malha na superfície external. O programa *ANSA* versão 19 da *Beta CAE Systems* foi utilizada para essa etapa, e o padrão de malha triangular STL representou geometria externa, totalizando 14 milhões de elementos *shell*. Tal malha foi exportada no formato *nastran* para a aplicação *PowerCASE* versão 5.5b, da empresa *Dassault Systemes*. Esse software tem como base o modelo de *Lattice-Boltzmann,* o qual usa a formulação *LES* (*Large Eddy Simulation*). Nele, as condições de contorno são aplicadas, tais como velocidade do fluxo de ar (50km/h e 100km/h),

tamanho do domínio computacional (domínio aberto sem influência das paredes, cujo tamanho é de 125m e comprimento, 85m de largura e 40m de altura, e também o domínio com dimensões semelhantes do túnel de vento da General Motors, cuja dimensões são 14m de comprimento, 12m de largura e 6m de altura), perda de carga nos trocadores de calor, velocidade de rotação das rodas, altura do modelo em relação ao chão, dentre outros. O parâmetros citados acima compreendem a simulação inicial de aerodinâmica: anteriormente a simulação de contaminação, uma simulação de aerodinâmica (apenas com uma fase de fluido, ar), é realizada como ponto inicial da simulação de contaminação e também para se compreender o comportamento do fluxo de ar ao redor do modelo. Tal simulação é realizada em duas etapas: uma inicial com a malha mais grosseira (menor elemento volumétrico na malha de 10mm de largura), a qual representa 10s de simulação transiente; a última iteração dessa primeira etapa alimenta uma simulação com malha mais refinada (malha padrão de 2.5mm de largura do menor elemento volumétrico, totalizando cerca de 90 milhões de *voxels* – elementos volumétricos). Essa etapa da simulação com malha refinada é de 2.0s de simulação transiente. Como a simulação é do domínio temporal, uma média do último segundo do tempo da simulação é feita para medir o coeficiente de arrasto aerodinâmico.

O custo computacional é contabilizado em termos de horas de rodagem da simulação vezes o número de *CPUs* utilizados para aquela simulação em específico (*CPUxH*). Em todos os casos apresentados nesse estudo, foram utilizados 288 *CPUs* por simulação e o tempo de rodagem nesses *CPUs* para as simulações de aerodinâmica foi em média de 24h, de forma que o custo computacional foi de 7000 *CPUxH*.

A última iteração da simulação de aerodinâmica é usada para iniciar a primeira iteração de contaminação, seja ela para o caso de chuva ou de auto-contaminação. Para ambos os casos, as condições de contorno da simulação de aerodinâmica foram aplicadas e as ferramentas de contaminação foram habilitadas. Para o caso de auto-contaminação, as condições de contorno foram semelhantes a simulação aerodinâmicas, porém, adicionando-se dois emissores de água, um na frente e outro atrás de cada pneu, tangenciais à superfície do pneu e próximo a região de contato do pneu com o chão (detalhes na Figura 16 do primeiro artigo). Essa posição é de certa forma diferente da posição em que o teste no túnel de vento aconteceu, mas representa um caso mais realístico de um veículo passando por uma estrada de terra ou neve. A vazão de cada emissor foi de 3.8L/min para a velocidade de 100km/h e ajustado dependendo da velocidade do veículo. Juntamente com o estudo da variação de velocidade (50km/h e 100km/h), a vazão de água foi estudada (metade o valor da vazão e o dobro), assim como o resolução da malha volumétrica (reduzindo o menor *voxel* 2.5mm pela metade do tamanho e dobrando o tamanho

do *voxel*). Por fim a distribuição e tamanho de partículas foram estudos, partindo o valor inicial de 0.165mm e distribuição uniforme para o dado experimental medido por Strohbucker et al. (2019) de 0.2mm e distribuição gaussiana com desvio padrão de 0.05mm.

Para o caso da simulação de chuva, os dois tipos de domínios mencionados anteriormente foram usados (domínio aberto e sessão de teste do túnel de vento) para assegurar que o domínio não afetaria o resultado de contaminação no vidro traseiro. Um duto foi modelado, com as mesmas dimensões do duto usado no teste do túnel de vento, de 1 polegada de diâmetro, uma vez que esse altera o fluxo de ar sobre o carro. O fluido considerado na simulação foi água e os emissores de água foram posicionados da mesma maneira que o teste do túnel de vento: três emissores, localizados a 0.75m de distância do chão e também a 1.1m de distância do chão, em diferentes simulações, mas sempre a 1.5m de distância do carro e na direção oposta ao fluxo de ar. A vazão de água também foi de 7.2L/min e o cone de abertura dos emissores de água foi de 9.6º e também de 65º, para estudar o impacto no resultado dessa variável.

As simulações de contaminação, por terem uma outra fase envolvida e por serem avaliadas por um tempo maior que as simulações aerodinâmicas (5s de tempo de simulação), apresentaram um custo computacional maior (cerca de 17000 *CPUxH*).

Para o estudo realizado no terceiro artigo, no qual a influência do ângulo de inclinação do vidro traseiro no coeficiente aerodinâmico e na contaminação do vidro traseiro foi estudada, uma outra ferramenta foi utilizada nos modelos de malha exportados no formato *Nastran.* Essa ferramenta, chamada *PowerDELTA*, também da empresa *Dassault Systemes*, é encarregada de fazer os *morphs* na traseira do modelo, de forma que a malha é distorcida para se obter o ângulo de inclinação desejado. A região da tampa do porta malas é restringida e a região do bordo de fuga do teto do carro pode ser movimentada, variando o ângulo de inclinação.

Na sessão de pós-processamento de resultados da simulação aerodinâmica, planos coloridos por velocidade foram utilizados para regiões de separação do fluxo de ar, bem como regiões volumétricas encapsulando o coeficiente de pressão total igual a zero. Essa última metodologia de visualização do fluxo de ar facilita a identificação das regiões de baixa pressão e onde tipicamente a separação do fluxo de ar ocorre na superfície. Para as simulações de contaminação, a espessura do filme de água sobre a superfície foi plotada e essas imagens foram utilizadas para comparação qualitativa da contaminação no vidro traseiro. A fim de comparar quantitativamente, uma metodologia foi criada, chamada de Índice de Contaminação. Tal índice consiste na densidade de partículas em uma determinada área com espessura de filme de água acima de 0.001mm. Portanto, em um caso hipotético, se um quarto da área do vidro traseiro possuir partículas acima de 0.001mm, o índice de contaminação será de 25%.

3 INTRODUÇÃO

Este trabalho apresenta uma sequência de três artigos sobre contaminação no vidro traseiro de veículos automotivos, utilizando túnel de vento climático e simulações numéricas. O termo contaminação é definido e mostra-se a importância do tópico atualmente. Também é apresentado como a contaminação pode variar dependendo de parâmetros geométricos e não geométricos.

O primeiro artigo com o título "*VEHICLE REAR END CONTAMINATION COMPARISON USING NUMERICAL SIMULATION AND WIND TUNNEL TEST*" representa o Capítulo 2 desta dissertação e foi submetido à revista *Journal: International Journal of Multiphase Flow* (fase *submetido*). Neste artigo é apresentada uma introdução ao termo contaminação numa esfera automotiva e como esse tópico tem se tornado cada vez mais relevante devido possibilidade de prever numericamente a contaminação em diversas áreas de veículos em fases conceituais do desenvolvimento.

Também são mencionadas ferramentas de engenharia para estudar contaminação e duas dessas ferramentas, túnel de vento climático e simulação numérica são utilizadas nesse artigo: inicialmente testes físicos em túnel de vento climático e em seguida, simulações numéricas para correlação.

Uma vez validada as simulações numéricas multifásicas transientes com a técnica *Lattice-Boltzmann* com o modelo físico em escala real testado em túnel de vento, deu-se continuidade ao estudo com modificações geométricas que influenciam a contaminação no vidro traseiro.

A primeira modificação estudada foi a presença de um *spoiler* no teto de um carro *hatch back* comercial (Chevrolet Malibu Maxx 2005). Esse foi o conteúdo do segundo artigo com título "*CASE STUDY OF VEHICLE BACK GLASS CONTAMINATION WITH AND WITHOUT SPOILER*" a ser submetido à revista *Journal: International Journal of Multiphase Flow* (fase *a ser submetido*), pelo qual foi possível determinar qual dos dois casos é mais crítico para contaminação no vidro traseiro: chuva ou sujeira de estrada, chamada de auto-contaminação.

No terceiro artigo, com título "*STUDY OF THE REAR BACKLIGHT ANGLE INFLUENCE ON VEHICLE AERODYNAMICS AND CONTAMINATION*" apresentado na WCX™ World Congress Experience - SAE International (doi:10.4271/2020-01-0691), foi estudado a influência do ângulo de inclinação do vidro traseiro na contaminação do mesmo.

Sabe-se de outros estudos da literatura, que esse parâmetro influencia o coeficiente de arrasto, portanto neste trabalho é comparado a influência do ângulo de inclinação do vidro traseiro tanto no efeito aerodinâmico (coeficiente de arrasto) quanto na contaminação.

4 ARTIGO 1: VEHICLE REAR END CONTAMINATION COMPARISON USING NUMERICAL SIMULATION AND WIND TUNNEL TEST

Abstract

This paper examines the rear contamination on a production vehicle comparing the results from physical test and numerical simulations. The physical test was performed in a climate wind tunnel using ultra-violet lights to visualize the water flow while a highly-resolved time accurate 3D computational fluid dynamics simulations were performed using a commercial Lattice-Boltzmann solver. This work focused on the back glass contamination, which is a driver to determine if a vehicle needs or not the rear wiper and a production fast back car was selected for the study due to its rear aerodynamic wake unsteadiness. Two load cases were evaluated in this paper, such as the wind-driven rain (regular rain) and self-soiling (effect of a car driven on a dirty road). Both were evaluated in the wind tunnel tests and CFD simulations, varying some parameters to study the results dependency. The results showed that simulation tools can be used to predict back glass contamination for the self-soiling case, but some special treatment is required for the wind-driven rain case due to gaps between exterior panels, not represented typically in CFD models. When the gaps were eliminated on the real car, the numerical simulation results got similar to the physical test results.

Introduction

Contamination is a very broad subject where it is studied how, when and where a non-desired object was introduced in a given domain. In the automotive world, contamination can be analyzed for engine intake (water ingestion for example), electrical components, brake performance, safety, vehicle's aesthetics, driver's vision as described by Hagemeier et al. [1] and many other areas. Gaylard et al. [2] also describe contaminant as "any substance foreign to a particular vehicle surface and degrades the vision of drivers, the visibility of vehicles, system performance or aesthetic appeal". The three main contamination sources, according to Kuthada et al. [3] are: primary-contamination (wind-driven rain), foreign-contamination (from car ahead) and self-soiling (mist and dirt particles from the tire kick up) (Figure 1). In a real case,

those contaminants could be water (rain), mud, snow, salt or other substance that could soil the vehicle surface. This paper focuses on the study of the self-soiling (vehicle gets dirty when driven on dirty road) and wind-driven rain (regular rain) load cases (Figure 2) on the back glass area.

Figure 1. Self-soiling phenomenon

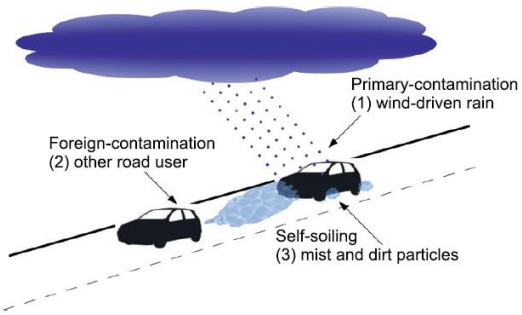

Figure 2. Three different origins for vehicle contamination: rain, foreign contamination and self-soiling [3]

Back glass contamination is a big concern especially for hatchbacks, station wagons, sport utility vehicles or any other squared back vehicle, where there is a massive airflow separation at the roof trailing edge. The low pressure bubble retains the contaminants from the tire spray as shown in Figure 3 and the surfaces with relatively higher pressure (back glass), get contaminated [2]. As described by Oliveira et. al [18], the same issue does not happen for sedans due to the backlight angle: if the airflow is still attached to the backglass, the low pressure bubble with the contaminants is below the decklid, keeping the particles away from the backglass (Figure 4). However, the water droplets of rain cases are airborne which means they will get in contact with the back glass for the sedans type of vehicle, increasing the

contamination at the area. The common enabler used by car manufactures to remove debris from the backglass is the rear wipers.

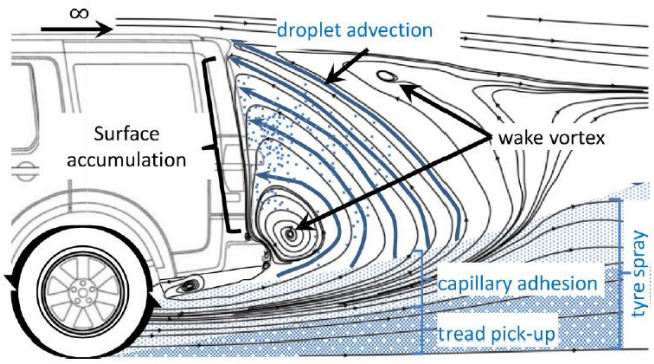

Figure 3. Schematic of rear surface contamination mechanisms on square back vehicles [17]

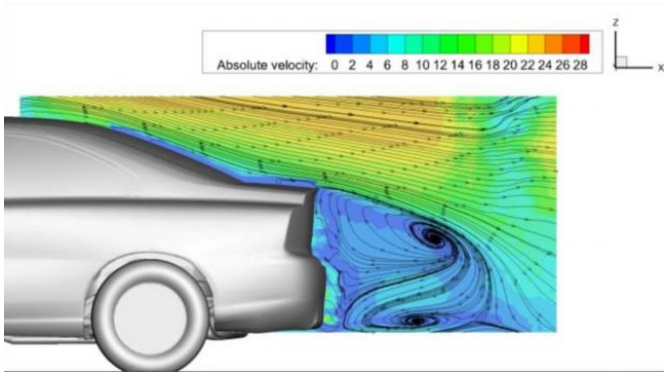

Figure 4. Low pressure bubble after the decklid trailing edge, showing where the contaminants are recirculating on a notchback vehicle [20]

Rear wipers are widely used on squared back vehicles, but not so common on notch back vehicles due to the distinguished aerodynamic behavior described above. The challenge occurs for fast back vehicles, which is an intermediate backlight angle condition, where may need or not rear wiper to clean the back glass. Example from the old to the new generation of the Nissan sport car: the rear wiper was removed from the vehicle (Figure 5 and 6). One of the reasons might be due to a cost and mass reduction and probably because the customers did not use the rear wiper so often once the back glass is clean most of the time. That was probably a conservative decision for the 2006 generation but it was an enhancement for the 2019 model year.

Figure 5. 2006 Nissan 350z with rear wiper

Figure 6. 2019 Nissan 370z without rear spoiler

Nowadays, there are four methods of investigating this contamination issues: driving on-road, driving on proving ground, wind tunnel testing or numerical simulation. Each of those methods has their own advantages and drawbacks, showed by Gaylard et al. [14].

Driving on-road is the most reliable method to get real data, however it requires a real vehicle, which happens by the end of the development process and usually cannot be revealed before the vehicle's official launch. Besides that, that method doesn't use a controlled environment, where repeatability is an issue. Driving on proving ground provides a secured and controlled environment, however it also required a full functional prototype to be tested. That disables design changes early on in the development process, which are cheaper than later changes. Wind tunnel testing can be performed early enough in the development process in order to make design changes in reasonable costs. This method also provides repeatability and security, being an excellent method to take decisions. However, as shown in this report, the cutline and body panels gaps are important to represent the correct physics and usually can't be represented in full size clay models, besides the wind tunnel hours to test are expensive. The numerical simulation method is based on Computational Fluid Dynamics (CFD) tool that can simulate fluid flow behavior using high-speed computers. There are well-known mathematical equations that represent how air and gases behave (Conservation of Mass, Momentum and Energy). These equations are extremely complex (differential equations), thus normally cannot

be solved by hand calculations. As computer power increased in the 1970s, the aerospace industry led the way in developing software to approximate solutions to these equations for complicated flows around aircraft and spacecraft. Over the past few decades, these software tools have advanced to a point where accurate solutions can be obtained for complex flows, including coupling particles and surface film models with time-accurate transient solutions [19]. The simulation method is a great method to make comparison between design changes, presents a quicker turn around compared with the wind tunnel method where a physical model has to be built, it is cheaper than wind tunnel hours and it can plot several quantities on a surface, enabling to investigating the root cause of the issues.

The purpose of this study is to compare back glass contamination using two methods described by Gaylard et al. [14]: wind tunnel and CFD, and evaluating in two different sources of contamination: wind-driven rain and self-soiling . Both cases were tested at General Motors Climate Wind Tunnel (in Warren, MI – USA) and simulated using the commercially available Lattice Boltzmann (LBM) CFD code, Dassault System PowerFLOW. With the results of this study, it will be possible to use numerical simulations to determine the need of rear wiper for future project.

As mentioned previously, notchback and squared back vehicles have very distinguish aerodynamics behaviors, where the presence or absence of rear wiper is well-known by the auto industry. Therefore, a fast back vehicle was selected for this study: 2015 Chevrolet Volt 2nd generation (Figure 7) which does not present a rear wiper.

Figure 7. 2015 Chevrolet Volt 2nd generation – fast back vehicle

Wind Tunnel Test Configuration

It was used the Climatic Wind Tunnel from General Motors in Warren, MI – USA to run this experiment (Figure 8). The facility can provide air temperatures from -40°C to +60°C, 5% to

95% relative humidity and with wind and road speeds up to 240km/h. It also has four belts to spin the wheels and the test section length of 13m. This tunnel is used to evaluate full size models on thermal, powertrain cooling and contamination tests and it was used in some other publications [22, 23].The focus of this study is the rear glass contamination and based on the study performed by Gaylard et al. [14], the rear wheels are the main contributor for the back face contamination. Thus, only the rear belts were turned on to spin the rear axle of the vehicle (Figure 9).

For contamination wind tunnel tests, the post-processing method to visualize the water flow is the fluorescence method, considered the state-of-the-art by Shilling et al. [26]. That method was first used by Kuthada et al. [27] in 2004 and consists in mixture of water and dye, which can be easily visualized by fluorescence lights in the dark. Some enhancements on that method was introduced lately, described by Shilling et al. [26] and Spruß et al. [28], where an automated post-processing tool measure the contamination quantitatively.

In this study, the traditional fluorescence method was adopted and using three nozzles Lechler 502-548 full-cone type and rated approximately 7.2 L/min at 2.75 bar. Upon powering the system, the pump starts and the recirc valve opens, filling the lines and circulating the mixture of 10% volume of water and 1% volume of chalk-powder. That mixture of water and dye is used to visualize the water flow under ultra violet lights. Pressing the start button opens the spray valve and closes the recirc valve, spraying the mixture for the duration that was set on the timer relay. The system then returns to recirc mode until the next cycle or power is turned off. For the wind tunnel test, the duration of each cycle was set to 80s and it was

performed low and high air speeds (50 km/h and 100 km/h) for each run. Figures 10 and 11 show the rake where the three nozzles were attached and the fluid circuit respectively.

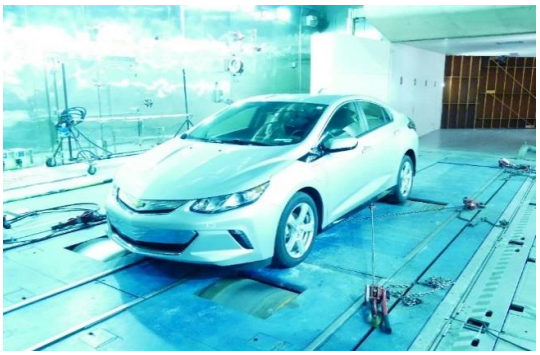

Figure 8. Model installed in the wind tunnel

Figure 9. Rear wheels on the belts to spin

Figure 10. Three nozzles on the rake

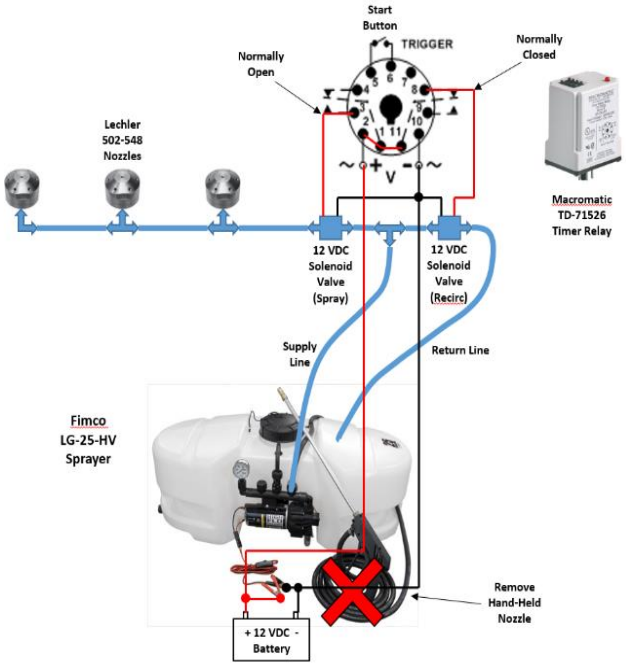

Figure 11. Schematic of the emitter circuit

Self-soiling Setup

The self-soiling runs were setup in two different ways. The first one the nozzle was positioned in front of the rear tire as shown in Figure 12. The same method was used by other authors, such as Strohbucker et al. [21]. In the alternative method, the nozzle was positioned behind the rear tire to understand the differences on the back glass contamination. One of the physical test limitation in this case was the length of the rake and the nozzles distribution on it: the rake was not long enough to cover both rear tires, so only the rear left tire had the emitter spraying fluid as seen in Figure 14, which means contamination on the rear end of the vehicle will not be symmetric and only the left hand side should be analyzed.

It was performed in total four run on the self-soiling case: nozzle in front of the rear left tire at 50km/h and 100km/h and nozzle behind the rear left tire at the same speeds.

Figure 12. Typical nozzle position in front of the rear tire: 0.13m from the ground and 0.23m from the front of the rear left tire

Figure 13. Alternative method: nozzle position behind the rear tire: 0.17m from the ground and 0.17m from the back of the rear left tire

Figure 14. Nozzles distribution on the rake

Wind-Driven Setup

The wind-driven rain runs were setup with the rake in front of the vehicle (1.5 m from the nose of the car) and different heights from the ground: initially at 1.5m, 1.1m and 0.75m. The nozzles sprayed the mixture in the opposite direction of the flow at a rate of 7.2 L/min and air speeds of 50 km/h and 100 km/h for all rake positions (Figure 15).

Figure 15. Wind-driven rain wind tunnel setup

Numerical Simulation

Aerodynamics Simulation

In the past, contamination simulations were not well developed as it is nowadays, and vehicle development relied mainly on hardware tests. Currently, Computational Fluid Dynamics (CFD) tools can simulate fluid flow behavior for complex flows, including coupling particles and surface film models with time-accurate unsteady solutions [10]. The Lattice-Boltzmann Method, implemented in the commercial software PowerFLOW, was used for the simulations presented in this paper. Jilesen et al. [8] describes the LBM method as the following: it is an inherently unsteady Lattice Boltzmann (LB) solver which uses what is essentially a Very Large Eddy Simulation (VLES) turbulence model.

The aerodynamic simulation setup used here followed lattice resolution and boundary conditions published in the PowerFLOW best practices for this type of vehicles (PowerFLOW user's guide v5.5a [23]). This computational code was used in many other publications, such as Jilesen [8, 9] and Gaylard [14]. It considered moving ground, with all four wheels were spinning

and the walls were 45m from the vehicle, which can be considered as an open domain (no influence of the side and top walls).

Contamination Simulation

Once the Aerodynamic simulation setup is completed, the Particle Modeling tool is turned on, which enables a film solver based on a Lagrangian particle simulator. The calculator assumes that particles form a thin film of fluid, which moves by the shear stresses. This simulator is formed by the splash model (studied by Mondo et al. [11] and O-Rourke and Amsden [12]), breakup model (specified by O-Rourke and Amsden [13]) and the re-entrainment model (which is defined by Jilesen et al. [8] as a critical film thickness of 0.3mm). Gravity is also included and causes acceleration on the film of fluid, such as dripping. The resultant film momentum equation is:

$$\rho h \frac{D\vec{u}}{Dt} = -2\mu \frac{\vec{u}}{h} + \vec{\tau}_{air}(\vec{u}_*, \vec{n}) + \rho(\vec{g} - (\vec{g} \cdot \vec{n})\vec{n})h \quad (1)$$

where ρ is the density of the film, h is the film height, $\vec{u}$ is the film velocity, μ is the film viscosity, $\vec{n}$ is the surface normal, and $\vec{g}$ is the acceleration due to gravity. The shear stress resulting from the air moving over the film, τair, is dependent on the near wall air velocity, $\vec{u}*$, and is provided by the flow solver (Jilesen et al. [8]).

The two-way coupling enables the energy conservation for each particle. That is used to predict the trajectory of each particle, since they have their local drag force and momentum. The resultant reactionary force acting on the surrounding air is also considered. The equation for the particle acceleration is:

$$m \frac{D\vec{u}_{Particle}}{Dt} = \frac{1}{2}\rho C_D A(\vec{u}_{Particle} - \vec{u}_*)|\vec{u}_{Particle} - \vec{u}_*| + m\vec{g} \quad (2)$$

where m is the particle mass, $\vec{u}$ is the particle velocity, CD is the drag coefficient for the particle, and A is the cross sectional area of the particle (Jilesen et al. [8]).

The coupling between the Lagrangian particle simulator with PowerFLOW allows millions of particles to be tracked simultaneously.

The CFD simulation used in this study included the particle splash, breakup, re-entrainment, two-way coupling between continuous (air) and dispersed (water) phases and all

four wheels spinning. The two-way particle-air coupling and wheel rotation were proved to be an important consideration to represent the correct physics, as demonstrated by Gaylard et at [14]. The one-way coupling does not enables the momentum transfer between the two phases, while the two-way coupling does.

A splash model was considered when liquid particles hit a surface, where these particles created child particles. The breakup model estimates when the aerodynamic shear causes a critical internal vibration to make a droplet to break-up and then splits the particle into child particles. The re-entrainment model calculated when the particle releases from a surface film: it allowed liquid to move along a surface, pool and re-enter the airflow as larger droplets. Jilesen et al. [9] describes each model in greater detail. The liquid density was (ρ) 1000 kg/m^3; dynamic viscosity was (μ) 1×10^{-3} Pa.s, and surface tension was (γ) 72.8×10^{-3} N/m.

Self-Soiling Setup

For the self-soiling simulation, two tire emitters at the angle of 29.5 degrees and 326 degrees (Figure 16) were configured for each tire. The nozzles in PowerFLOW represent the bounds of the emitter that sits on the surface of the tire. Particles are emitted from the entire tire because water can fly off the tire at any point in its rotation. A standard deviation of 5 m/s was added and dripped particles larger than 0.3mm were re-entrained into the airflow. This simulation setup was based on PowerFLOW best practice and verified by Jilesen et at. [9]. The setup also included the vehicle speed at 100 km/h, water flow rate of 3.8 L/min and particle diameter of 0.165mm [8] (represents 1mm of water film on the road).

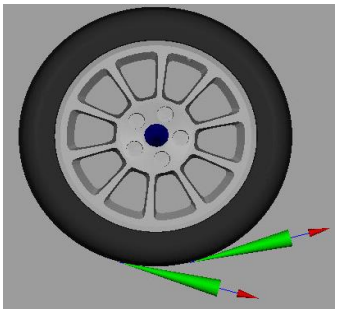

Figure 16. A schematic of tire emitter for self-soiling

The lattice refinement was defined as shown in Figure 17. The coarsest element size on the top of the Figure 17 was 50mm and the finest element size closer to the vehicle surface was

2.5mm. The number of volumetric elements in each case was around 90 million. To ensure the mesh resolution will not affect the contamination simulation results, a mesh size study was performed in another model [18]. The aerodynamic simulation lattice size (Figure 17) was taken as the baseline and a coarser (double of the baseline lattice size – Figure 18) and finer (half of the baseline lattice size – Figure19) lattice results were evaluated.

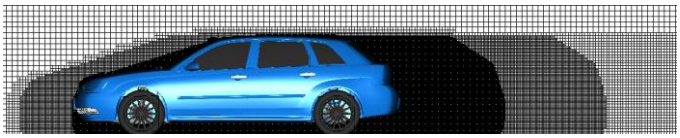

Figure 17. Baseline Lattice Resolution

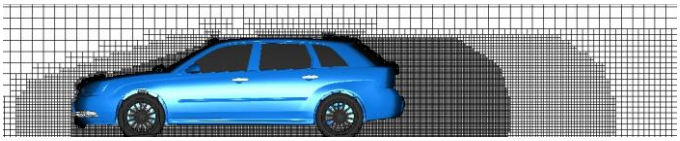

Figure 18. Coarser Lattice Resolution

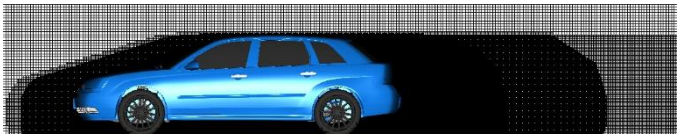

Figure 19. Finer Lattice Resolution

In order to objectively measure the back glass contamination, Oliveira et al. [18] proposed the Contamination Index, defined as "the number of particles greater than $1x10^{-6}$m on a determined surface (similar to a density). For example, if 25% of the interested area is cover by film thickness larger than $1x10^{-6}$m, the Contamination Index is 25%". The results of the mesh resolution study described above can be observed in the Figure 20, 21 and 22: film thickness quantity is plotted on the model surface to study the contamination on the back glass. The computational cost (run time in CPUxHours) and the contamination index on back glass area are also compared among the lattice resolution study. Based on the contamination index, simulation cost and film thickness plot, it was defined to use the baseline aerodynamics lattice for the following simulations: back glass is clean on the higher resolution mesh and the baseline mesh but baseline mesh is cheaper from a computational standpoint.

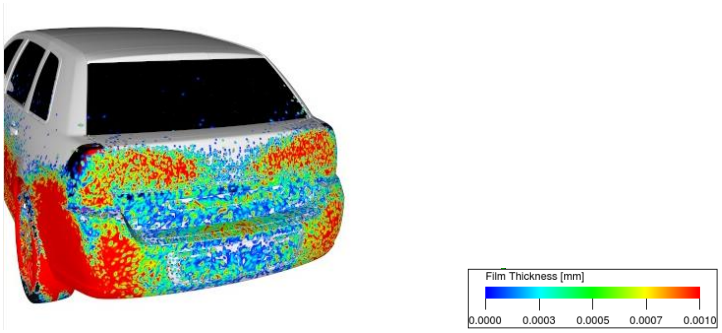

Figure 20. Film Thickness Plot using Baseline Lattice Resolution: Contamination Index on back glass area of 0.1% and 17k CPUxh

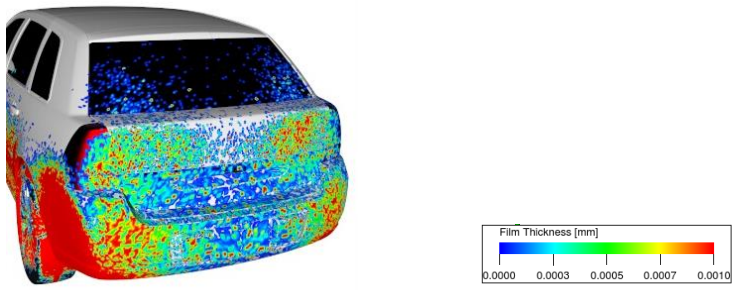

Figure 21. Film Thickness Plot using Coarser Lattice Resolution: Contamination Index on back glass area of 0.3% and 8.5k CPUxh

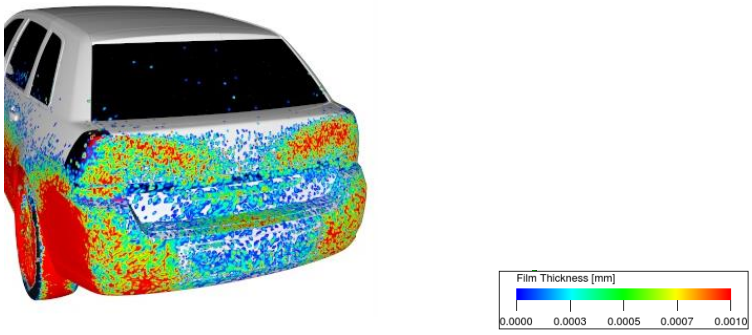

Figure 22. Film Thickness Plot using Finer Lattice Resolution: Contamination Index on back glass area of 0.0% and 40k CPUxh

Another parameter studied was the emitter rate: as previously mentioned, PowerFLOW recommends water flow rate of 3.8 L/min per emitter, therefore, half and double of the emitter rate were evaluated. Contamination index around 0% was observed for all cases and film thickness distribution presented similar pattern: thicker film thickness on the tail gate corner

(Figure 23). Based on this result, it concludes the emitter rate changes the speed to reach steady state, but not the actual contaminants distribution on the surface. Gaylard et al. [22] observed the accumulation of mass is linear with time and the "relative distribution changes little as the simulation progress, implying that shorter simulations can be compared to longer experiments. Further the rate of accumulation quickly reaches a settle mean value, suggesting utility as a metric for assessing different vehicles". Then the baseline emitter rate was considered for future runs.

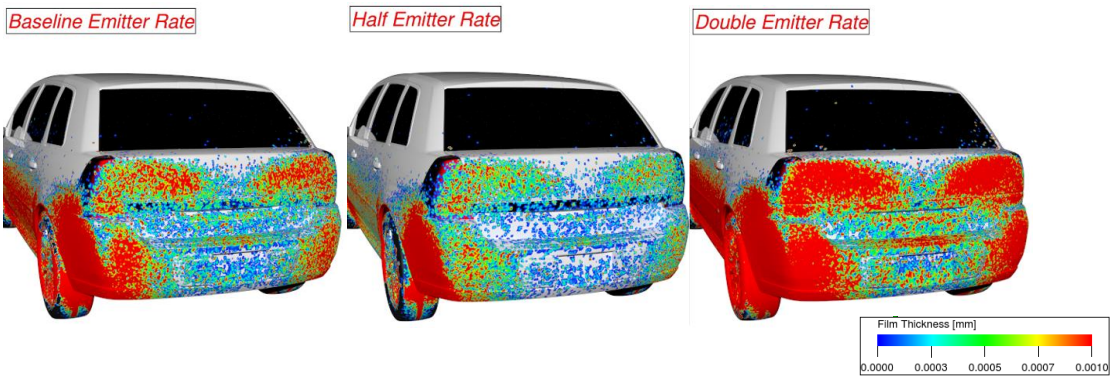

Figure 23. Film Thickness Plot varying the emitter rate

A very similar trend was observed when the vehicle speed was studied. The model used for that study was the same front end of the previous model studied so far, but using a morphed backlight angle to represent a squared back vehicle. 50km/h and 100km/h vehicle speeds were simulated and presented 6% and 51% contamination index on the back glass respectively. The higher speed case promotes a to achieve thicker film thickness during the same 5s of simulation time without changing the contamination pattern, then it was used the 100km/h to perform future runs. Gaylard et al. [2] studied the tire rotational speeds and concluded that for higher speeds, more particles break-up happens, which will reach the vehicle surface (Figure 24).

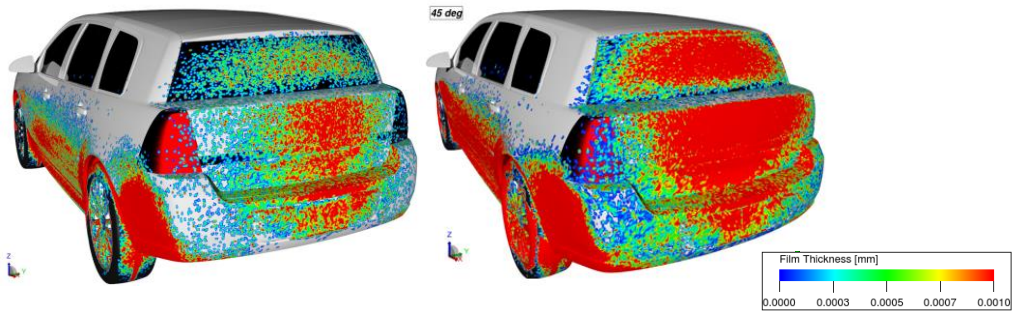

Figure 24. Film Thickness Plot varying the vehicle speed: 50km/h at the left and 100km/h at the right

The last study performed on the self-soiling baseline setup was on the particle size and distribution: the simulations done so far used particle diameter of 0.165mm and uniform distribution presented by Jilesen et al. [8]. Strohbucker et al. [21] recently measured the particle size and distribution based on experimental wind tunnel data (Figure 25). The results showed the majority of the particles diameter is 0.2mm and a Gaussian distribution with standard deviation of 0.05mm would be a recommended approach. Jilesen et al. [8] and Strohbucker et al. [21] particle configurations were compared using the simulation tool. The actual Volt model was evaluated on this study and the back glass contamination index was 0% on both and the film thickness pattern also very similar on both (Figure 26). Based on the study, Jilesen et al. [8] particle configuration was selected to run future analyses.

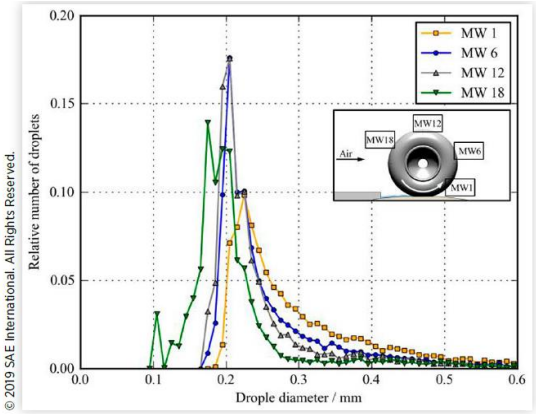

Figure 25. Droplet size distribution measured by Strohbucker et al. [21]

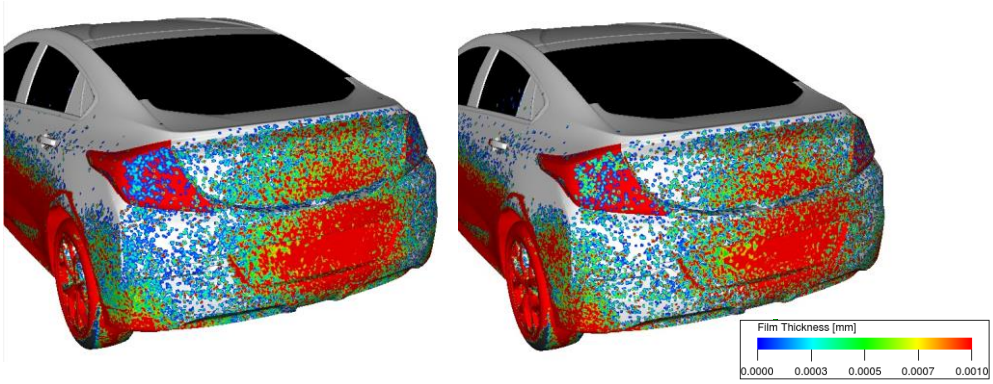

Figure 26. Film thickness plot using Jilesen (left) and Strohbucker (right) particle configurations.

Wind-driven Rain Setup

Some of the learning from the Self-soiling studies were applied to the Wind-driven Rain cases, such as the lattice resolution and vehicle speed selections. The domain used for the Self-soiling simulations was considered open domain (no influence of the side and top walls - walls 45m from the vehicle). However, for the Wind-driven Rain cases, the physical wind tunnel walls could influence the results, and then the facility test session was modeled in the simulation (Figure 27) to certificate that.

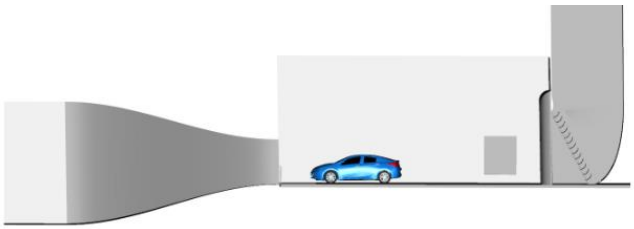

Figure 27. Wind Tunnel Walls considered in the simulation

Some other variables studied for the rain load case were the emitter type (same rake with nozzles and positions as the physical test and a box in front of the model was also considered, Figure 28), particle diameter (0.4mm and 2.0mm), water flow rate of 7.2 L/min, 17 L/min and 27 L/min. Table 1 summarizes each configuration studies focusing on the back glass film thickness.

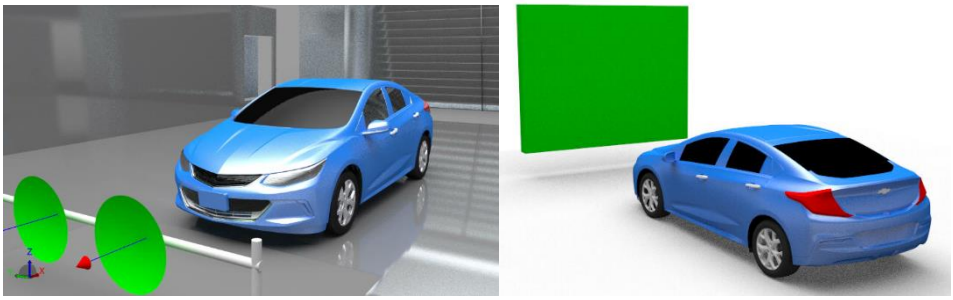

Figure 28. Different emitter types

Results

The first set of results shows the Self-soiling wind tunnel and the comparison with the simulation results and the second set of results shows the Wind-driven Rain wind tunnel and its comparison with the simulation results. Wind Tunnel results are pictures and videos showing the water accumulation on the rear end surface. The UV fluorescent lights glare is unfortunately displayed as well and it might make the data understanding more difficult. While the simulation results show the film thickness on the vehicle surface.

Self-Soling

The results are shown below: two wind tunnel emitter configurations (in front and behind the rear tires) and at 50km/h and 100km/h and the CFD results at 100km/h. The wind tunnel results have the emitter only at the rear left wheel, meaning the right hand side of the back panel will not get as contaminated .

Figure 29 – Emitter behind the rear left wheel: 50km/h at the left and 100km/h at the right

Figure 30 – Emitter in front of the rear left wheel: 50km/h at the left and 100km/h at the right

In the fig. 29 is presented self-soiling experiment with the emitter located behind the rear left tire: wind speed and wheels spinning at 50km/h at the left and at 100km/h at the right. In the fig. 30 is presented the same experiment, but with the emitter located in front of the rear left tire: wind speed and wheels spinning at 50km/h and 100km/h at the left and right pictures respectively. Based on the test results, it is possible to observe on both emitter setups that the higher speed runs presented wider water contamination on the tailgate and rear fascia, where they got saturated and started dripping before test time reaches the 80s. However, the emitters in front of the rear tires seem to be more realistic and the water distribution is slightly different from emitter behind the tire, due to the grooves effecting the water flow. According to Gaylard et al. [2], grooves change the water drainage and consequently the amount of water lifted, "releasing more spray higher up the rear face of the tire". In addition, the initial jet velocity coming from the emitter provides an artificial effect: in the emitter in front of the tire case, the jet is impinging the tire face while in the emitter behind the tire case, the jet gets an extra momentum if compared to a real tire splash.

Nevertheless, in all cases, the back glass was not contaminated at all (Figure 29 and 30), showing the methods were robust to study the backglass contamination.

With the purpose to compare the CFD data to wind tunnel data, Adobe Photoshop color saturation was used to highlight the water accumulation on the physical test (Figure 31 left). Saturation is the intensity of a color to be more vivid (higher saturation) or closer to gray (lower saturation). In that case, yellow color intensity was set as +100, while hue was set -35. The simulation result is show at Figure 32 right.

Despite the fact that tire tires representation was different between CFD (smooth tires) and wind tunnel test (real treaded tires), the self-soiling presented a very good correlation between the two tools. At higher vehicle speeds, 100km/h in this case, the rear contamination was greater on both tools due to the higher tires ’angular speed, kicking up more water and due to the larger aerodynamic wake structure. The major area of interest, the back glass, was cleaned on both tools while the center of the tailgate was the heavily contaminated area at the rear end. Another good area of correlation was the tail lamp: in Figure 32, the tail lamp on the real car seems to be clean, but when zoomed in, it is possible to see very small water droplets on it, represented by the 0.003mm film thickness in the CFD picture (at the right).

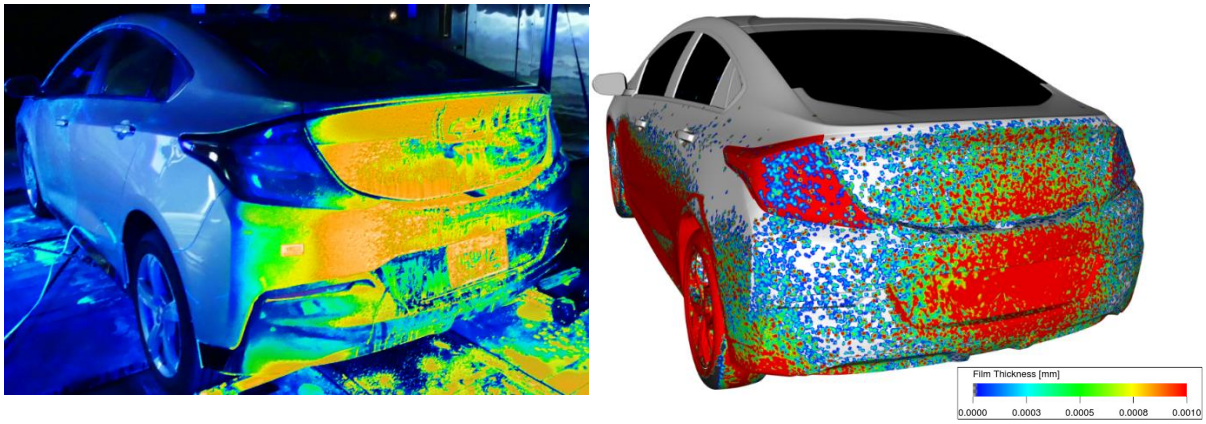

Figure 31 – Wind Tunnel picture (at the left) and CFD picture (at the right)

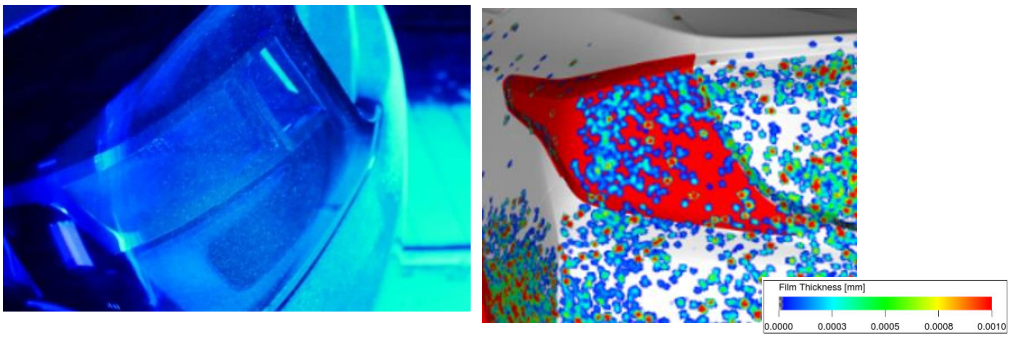

Figure 32 – Zoomed in Wind Tunnel picture (at the left) and Zoomed in CFD picture (at the right)

.

Overall, CFD results were able to precit the back glass contamination and rear faces also presented good correlation between the tool, despite the setup differences.

Wind-driven Rain

The rake with the nozzles emitting water was set in the opposite wind direction and in front of the car to promote a homogeneous water cloud onto the car. The rake height was set based on a live video of the rear of the car: the goal was to watch the airborne water flowing surrounded the back glass. The initial height was 1.5m to the ground, but the water wake was not englobing the entire back glass (Figure 33 left), then it was set to 1.1m to the ground and the water rake was observed at the back glass (Figure 33 right).

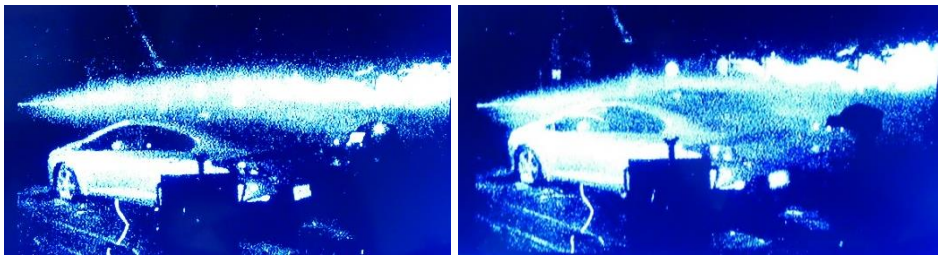

Figure 33 –Wind Tunnel picture with emitter rake at 1.5m (at the left) and 1.1m (at the right) from the ground

The results of the back glass contamination can be seen in Figure 34: back glass did not present any water droplet, surprisingly; even with the front end being completely wet (Figure 35). To ensure the rake height was not the issue, a lower height was tested (0.75m from the ground), but the back glass result was identical.

The reason is shown in Figure 36, where the gaps between the panels and B-side gutters drained the water from the back glass. Because of that, the gap in the physical model roof was tapped to confirm it was the actual reason of the unexpected results, which can be seen in Figure 37. With the roof gaps tapped, there was water flowing from the roof to the back glass, which confirms the initial assumption.

Figure 34 – Physical test results of Wind-driven Rain Test

Figure 35 – Physical test results of Wind-driven Rain Test

Figure 36 – Physical test results showing water running in the roof gaps

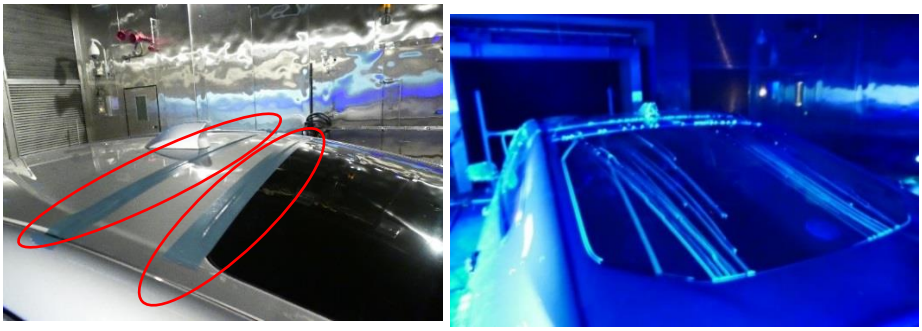

Figure 37 – Physical test results of Wind-driven Rain Test with roof gaps taped

As mentioned previously in the wind driven-rain simulation setup section, there are different domains (open domain and the actual wind tunnel domain), particle size, water rate and the emitter type (plane in front of the car and rake with nozzles) which were studied. The summary can be seen in the table 1.

Configuration	Domain	Particle Size [mm]	Water rate [L/min]	Emitter Type	Visualization
1	Open	2	17	Plane	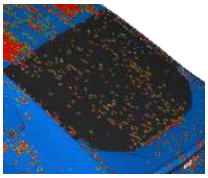
2	Open	0.4	27	Plane	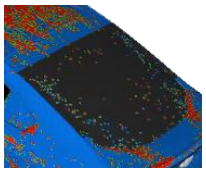
3	CWT	0.4	7.2	Rake in front of the car; 65deg nozzle half-angle; 0.75m from ground	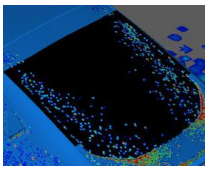
4	CWT	0.4	7.2	Rake in front of the car; 65deg nozzle half-angle; 1.1m from ground	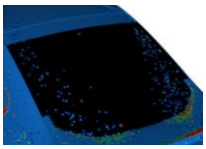
5	CWT	0.4	7.2	Rake in front of the car; 9.6deg nozzle half-angle; 1.1m from ground	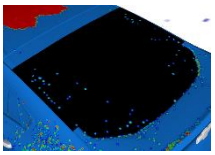

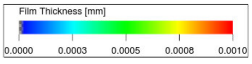

Table 1 – Wind-driven Rain Simulation Summary

The simulation results show the back glass is contaminated regardless the configuration method. When the Plane is used as the emitter, there is more water on the back glass comparing to the rake. The rake height did not change the distribution (concentration on the corners), but changed the film thickness intensity. Lastly, the nozzle angle also changes the film thickness intensity, but not the overall distribution.

When comparing the simulation with the physical test in the wind tunnel, it only can be compared the results with the taped on the roof gaps, since the simulation does not have the gaps representation in the model (Figure 38). The simulation model cabin is fully sealed while the real car has about 8mm gap between the panels, where water can flow though. Figure 39 shows the results between the roof taped in the experiment and the simulation (configuration 3 of Table 1): higher water concentration at the corners of the back glass on both tools. Another observation to the experiment methods is that the tape leading thickness creates a step to the flow, which can be another differentiation from the CFD model as well, but the overall results presented a decent comparison.

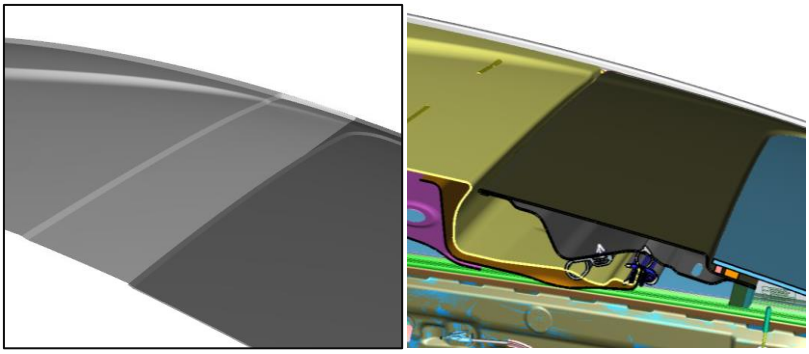

Figure 38 – Difference between CFD and Actual vehicle at the roof to back glass panels: gaps of 8mm

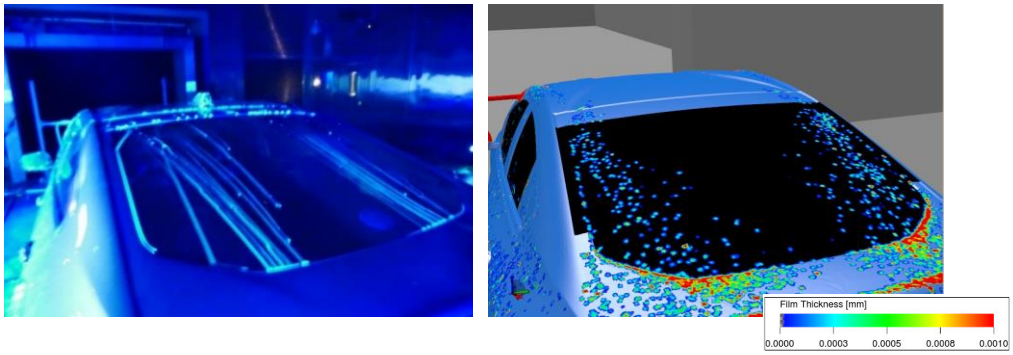

Figure 39 – Physical test results of Wind-driven Rain Test with roof gaps taped and CFD results at the right

In order to compare the wind tunnel and CFD results numerically, MATLAB was used as an image post-processing analysis tool, where the number of pixels were counted on the back glass area of each picture, real car test and CFD simulation (Figure 40 left and right respectively). The pixels highlighted in pink (water representation) were counted as well as the ones colored in green (area of the glass not contaminated) and the ratio between the area

occupied by the water and the total area was calculated for each image of the Figure 40. The physical test showed that 11% of the back glass area was covered by water and 7% in the simulation results. This method is not as accurate as the Contamination Index used for the self-soiling simulations, but it is acceptable to compare physical test results pictures taken at the same position, once the picture angle and glare can introduce noise into this method.

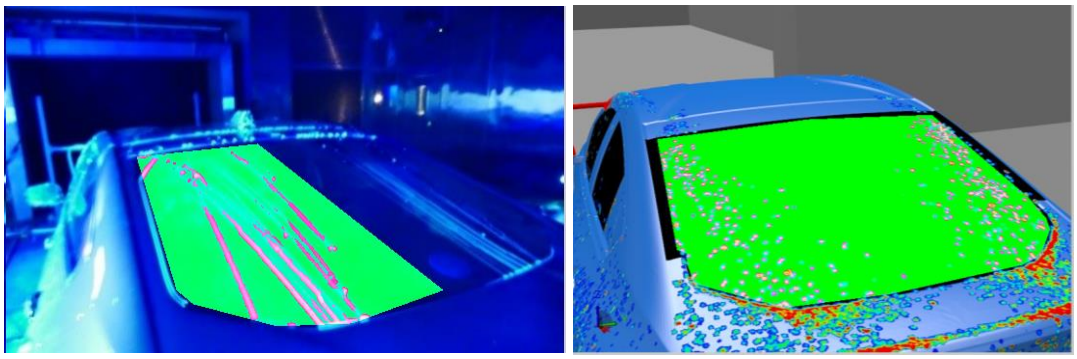

Figure 40 – Physical test results of Wind-driven Rain Test with roof gaps taped at the left and CFD results at the right

Conclusions

Based on the wind tunnel and simulation results, it concludes the simulation tool can be used to determine if the back glass will be contaminated, especially on the self-soiling case. Gaylard et al. [14] observed “a good qualitative comparison for contamination distribution” when comparing numerical simulations and wind tunnel tests. Some limitations was still observed in this study on the wind-driven rain case, where a more detailed CFD model is needed, representing the gaps between panels and B-side sheet metal), which may not exist in early development phases. In addition, a higher mesh resolution will be required to capture the gaps properly, making the simulation more expensive. The gaps study for the wind-driven rain simulation is a suggestion of future work, once the gaps matters on the back glass contamination.

References

1. Hagemeier, T., Hartmann, M., Thevenin, D., “Practice of vehicle soiling investigations: A review”, International Journal of Multiphase Flow, 37 (2011) 860-875, www.elsevier.com/locate/ijmulflow

2. Gaylard, A., Kirwan, K., Lockerby D., “Surface contamination of cars: A review”, in SAGE Journals, April 2017, doi:10.1177/0954407017695141.

3. Kuthada, T, Cyr, S. Approaches to vehicle soiling. In: 4th FKFS conference on progress in vehicle aerodynamics and thermal management: numerical methods (eds Wiedermann, J, Hucho, WH), Stuttgart, Germany, 2006, pp. 111–123. Renningen: Expert-Verlag.

4. Goetz, H., "The Influence of Wind Tunnel Tests on Body Design, Ventilation, and Surface Deposits of Sedans and Sport Cars," SAE Technical Paper 710212, 1971, https://doi.org/10.4271/710212.

5. Sims-Williams, D., Marwood, D., and Sprot, A., "Links between Notchback Geometry, Aerodynamic Drag, Flow Asymmetry and Unsteady Wake Structure," SAE Int. J. Passeng. Cars – Mech. Syst. 4(1):156-165, 2011, https://doi.org/10.4271/2011-01-0166.

6. Hucho, W. H., Janssen, L. J., Emmelmann, H. J., “The Optimization of Body Details – A Method for Reducing the Aerodynamic Drag of Road Vehicle “, in SAE Paper Nr. 760185.

7. Kabanovs, A., Hodgson, G., Garmory, A., Passmore, M., Gaylard, A., “A Parametric Study of Automotive Rear End Geometries on Rear Soiling”, in SAE Int. 2017, doi:10.4271/2017-01-1511.

8. Jilesen, J., Alajbegovic, A., Duncan, B., “Soiling and Rain Simulation for Ground Transportation Vehicles”, 7th European-Japanese Two-Phase Flow Group Meeting, 2015, Zermatt, Switzerland.

9. Jilesen, J., Gaylard, A., Duncan, B., Konstantinov, A. et al., "Simulation of Rear and Body Side Vehicle Soiling by Road Sprays Using Transient Particle Tracking," SAE Int. J. Passeng. Cars - Mech. Syst. 6(1):2013, doi: 10.4271/2013-01-1256.

10. Linfield, Kevin W., Mudry, Robert G., “Pros and Cons of CFD and Physical Flow Modeling”, Airflow Science Corporation, 2008. http://www.airflowsciences.com/.

11. Mondo, C., Sommerfeld, M., Tropea, C. (1995). “Droplet-wall collisions: Experimental studies of the deformation and breakup process” in Int. J. Multiphase Flow, Vol 21, pp. 151-173.

12. O'Rourke, P.J., Amsden, A. A. (2000). A spray/wall interaction submodel for Kiva-3 wall film model in SAE Paper Nr. 2000-01-0271.

13. O'Rourke, P.J., Amsden, A. A. (1987). The TAB method for numerical calculations of spray droplet breakup in International Fuels and Lubricants Meeting and Exposition, Toronto.

14. Gaylard, A., Pitman, J., Jilesen, J., Gagliardi, A. et al., "Insights into Rear Surface Contamination Using Simulation of Road Spray and Aerodynamics," SAE Int. J. Passeng. Cars - Mech. Syst. 7(2):2014, doi:10.4271/2014-01-0610.

15. Ahmed, S., Ramm, G., and Faltin, G., "Some Salient Features Of The Time-Averaged Ground Vehicle Wake," SAE Technical Paper 840300, 1984, https://doi.org/10.4271/840300.

16. Jilesen, J., Gaylard, A., and Escobar, J., "Numerical Investigation of Features Affecting Rear and Side Body Soiling," SAE Int. J. Passeng. Cars - Mech. Syst. 10(1):2017, doi:10.4271/2017-01-1543.

17. Gaylard, A. P. (2016, 30 Nov.) "rear_soiling_mechanism.emf," https://dx.doi.org/10.6084/m9.figshare.4270085.v1 with an access on Dec 2019.

18. Oliveira, D., dos Santos, R. G., “Study of the Effective Backlight Angle Influence on Vehicle Aerodynamics and Contamination”, SAE Technical Paper 2020-01-0691.

19. Linfield, Kevin W., Mudry, Robert G., “Pros and Cons of CFD and Physical Flow Modeling”, Airflow Science Corporation, 2008. http://www.airflowsciences.com/

20. Kounenis, Charalampos and Bonitz, Sabine and Ljungskog, Emil and Sims-Williams, David and Lofdahl, Lennart and Broniewicz, Alexander and Larsson, Lars and Sebben, Simone (2016) 'Investigations of the rear-end ow structures on a Sedan car.', SAE technical paper series. 2016-01-1606.

21. Strohbücker, V., Niesner, R., Schramm, D., Kuthada, T. et al., "Experimental Investigation of the Droplet Field of a Rotating Vehicle Tyre," SAE Technical Paper 2019-01-5068, 2019, doi:10.4271/2019-01-5068.

22. Gaylard, A. P.; Kabanovs, A.; Jilesen, J.; Kirwan, K.; Lockerby, D.A.; "Simulation of rear surface contamination for a simple bluff body", Journal of Wind Engineering and Industrial Aerodynamics, 2017

23. PowerFLOW products information website: https://www.3ds.com/products-services/simulia/products/powerflow/ (May 2020).

24. Best, S., Komar, J., and Elfstrom, G., "The UOIT Automotive Centre of Excellence - Climatic Test Facility," SAE Int. J. Passeng. Cars - Mech. Syst. 6(1):78-87, 2013, https://doi.org/10.4271/2013-01-0597

25. Chen, K., Bozeman, J., Wang, M., Ghosh, D. et al., "Energy Efficiency Impact of Localized Cooling/Heating for Electric Vehicle," SAE Technical Paper 2015-01-0352, 2015, https://doi.org/10.4271/2015-01-0352

26. Schilling, F., Kuthada, T., Gaylard, A., Wiedemann, J. et al., "Advances in Experimental Vehicle Soiling Tests," SAE Technical - Paper 2020-01-0681, 2020, doi:10.4271/2020-01-0681.

27. Kuthada, T., Widdecke, N., and Wiedemann, J., "Advanced Investigation Methods on Vehicle Soiling," in International Vehicle Aerodynamics Conference, 2004.

28. Spruß, I., Landwehr, T., Kuthada, T., and Wiedemann, J., "Advanced Investigation Methods on Side Glass Soiling," in Progress in Vehicle Aerodynamics and Thermal Management, 2013, 167-181.

Contact Information

Aerodynamics CFD Engineer at General Motors: danilo.oliveira@gm.com

Acknowledgments

The authors would like to thank General Motors for permission to publish this paper and especially some people who supported this work: Marcelo Bertocchi – GM CAE Director, Silvia Karlsson – GM Aerodynamics CFD Group Manager, Gena Vitale – GM Aerodynamics CFD Group Manager, Donnell Johnson – GM Aerodynamics Test Engineer, Fernando Saito – GM Aerodynamics Test Engineer, Flavio B Sales – GM Aerodynamics CFD, Danyang Fan – GM Aerodynamics CFD, Michael Demeo - Dassault System, Jeremy Beedy - Dassault System, Jonathan Jilesen - Dassault System, Timo Kuthada – FKFS.

5 ARTIGO 2: CASE STUDY OF VEHICLE BACK GLASS CONTAMINATION WITH AND WITHOUT SPOILER

Abstract

This paper presents contamination simulation results of a commercial vehicle with and without the roof spoiler. Highly-resolved, time accurate Computational Fluid Dynamics (CFD) simulations were performed using a commercial Lattice-Boltzmann solver, to compare the back glass contamination with those two configurations. In 2004, the Chevrolet Malibu Maxx was released without the roof spoiler and without a rear wiper. In 2005, a roof spoiler was added to the vehicle due to styling and aerodynamics reasons. Hence a rear wiper had to be added as well to mitigate some of the back glass contamination. The same phenomenon is predicted with numerical simulation tools in this paper. The contamination simulation results confirmed the newer model year vehicle needed a rear wiper in order to keep the backglass cleaned and also set a threshold curve to determine the need of rear wiper for future applications.

Introduction

Contamination is defined by Gaylard et al. [1] as the study of "any substance foreign to a particular vehicle surface and degrades the vision of drivers, the visibility of vehicles, system performance or aesthetic appeal". There are three main contamination sources, according to Kuthada et al. [2]: primary-contamination (wind-driven rain), foreign-contamination (from car ahead) and self-soiling (mist and dirt particles from the tire kick up, Figure 1). This paper studies the self-soiling and wind-driven rain load cases (Figure 2), focusing on the back glass area. Regarding contamination, the auto industry is mainly concerned on the with drivers' vision [3] (front, side and back glasses). However, other contamination issues on road vehicles are important, such as brake performance degradation, surface soiling (aesthetics), especially when driving on dirty, snowy or muddy roads. Lastly, sensors and cameras contamination around autonomous vehicles has become a very important topic in the auto industry, once those parts have to be clean for acceptable performance.

Figure 1. Self-soiling Condition

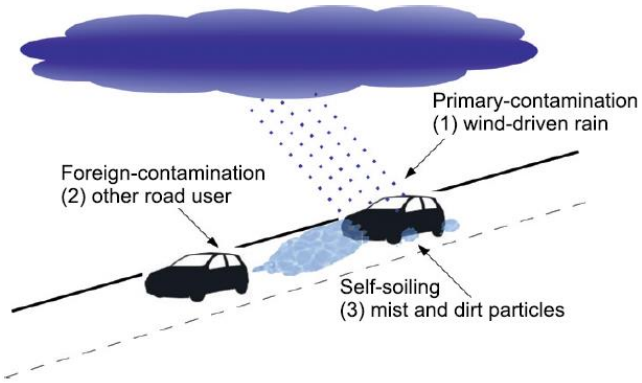

Figure 2. Three different origins for vehicle contamination: rain, foreign contamination and self-soiling [2]

To mitigate back glass contamination, usually car manufacturers use rear wipers or air deflectors: in 1989, GM implemented an air deflector on the Chevrolet Celebrity Station Wagon (Figure 3) as a back glass contamination countermeasure, but aerodynamic drag can increase up to 20% because of it, directly increasing fuel consumption [4].

Figure 3. 1989 Chevrolet Celebrity Station Wagon with air deflector to reduce back glass contamination.

In 2004, Chevrolet Malibu Maxx was released, shown in Figure 4 without a roof spoiler and without the rear wiper. In 2005, it was necessary to add a roof spoiler on this vehicle (Figure 5) due to styling and aerodynamics reasons. After some durability tests performed at the dirty roads on the newer model year vehicle, it was observed its back glass became dirty. To mitigate the issue, a rear wiper was added to keep the driver's vision standards acceptable.

Figure 4. 2004 Chevrolet Malibu Maxx (no spoiler and no rear wiper)

Figure 5. 2005 Chevrolet Malibu Maxx (spoiler and rear wiper)

The motivation of the paper is to study the contamination effects due to the addition of a roof spoiler on a commercial vehicle based on Numerical Simulation by comparing the back glass contamination with a model without spoiler.

Numerical Simulation

Aerodynamics Simulation

Compared to traditional wind tunnel tests, numerical simulations present quicker turnaround times, is cheaper to produce and enables in-depth investigations through the ability to plot and visualize multiple quantities on the vehicle surface. The Lattice-Boltzmann Method,

implemented in the commercial software PowerFLOW, was used for the simulations presented in this paper. LBM is a CFD technology based on kinetic theory and has been developed over the last 25-30 years. Jilesen et al. [5] describes the LBM method as the following: it is an inherently unsteady Lattice Boltzmann (LB) solver which uses what is essentially a Very Large Eddy Simulation (VLES) turbulence model.

The aerodynamic simulation setup followed mesh resolution and boundary conditions published in the PowerFLOW best practices for this type of vehicles (PowerFLOW user's manual). It considered air velocity of 100 km/h and moving ground. In that regular aerodynamic simulation, all four wheels were spinning and the walls were 45m from the vehicle, which can be considered as an open domain (no influence of the side and top walls).

The lattice refinement was defined as shown in Figure 6. The coarsest element size on the top of the Figure 6 was 50mm and the finest element size closer to the vehicle surface was 2.5mm. The number of volumetric elements in each case was around 90 million.

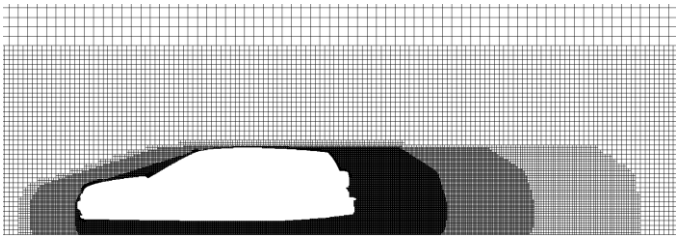

Figure 6. Volumetric Mesh Resolution

Contamination Simulation

In 2004 and 2005, when those studied cars were released, contamination simulations were not well developed as it is nowadays, and vehicle development relied mainly on hardware tests. Currently, Computational Fluid Dynamics (CFD) tool can simulate fluid flow behavior for complex flows, including coupling particles and surface film models with time-accurate unsteady solutions [6]. Gaylard et al. [1], Jilesen et al. [5 and 7] and many other authors, performed comparison between this commercial software and physical tests in wind tunnel.

Once the Aerodynamic simulation setup is completed, the Particle Modeling tool is turned on, which enables a film solver based on a Lagrangian particle simulator. The calculator assumes that particles form a thin film of fluid, which moves by the shear stresses. This simulator is formed by the splash model (studied by Mondo et al. [8] and O-Rourke and Amsden [9]), breakup model (specified by O-Rourke and Amsden [10]) and the re-entrainment model (which is defined by Jilesen et al. [5] as a critical film thickness of 0.3mm).

Gravity is also included and causes acceleration on the film of fluid, such as dripping. The resultant film momentum equation is:

$$\rho h \frac{D\vec{u}}{Dt} = -2\mu \frac{\vec{u}}{h} + \vec{\tau}_{air}(\vec{u}_*, \vec{n}) + \rho(\vec{g} - (\vec{g} \cdot \vec{n})\vec{n})h \quad (1)$$

where ρ is the density of the film, h is the film height, $\vec{u}$ is the film velocity, μ is the film viscosity, $\vec{n}$ is the surface normal, and $\vec{g}$ is the acceleration due to gravity. The shear stress resulting from the air moving over the film, τair, is dependent on the near wall air velocity, $\vec{u}*$, and is provided by the flow solver (Jilesen et al. [5]).

The two-way coupling comprehends the energy conservation for each particle. That is used to predict the trajectory of each particle, since they have their local drag force and momentum. The resultant reactionary force acting on the surrounding air is also considered. The equation for the particle acceleration is:

$$m\frac{D\vec{u}_{Particle}}{Dt} = \frac{1}{2}\rho C_D A(\vec{u}_{Particle} - \vec{u}_*)|\vec{u}_{Particle} - \vec{u}_*| + m\vec{g} \quad (2)$$

where m is the particle mass, $\vec{u}$ is the particle velocity, CD is the drag coefficient for the particle, and A is the cross sectional area of the particle (Jilesen et al. [2]).

The coupling between the Lagrangian particle simulator with PowerFLOW allows millions of particles to be tracked simultaneously.

Simulation Setup

The CFD simulation used in this study included the particle splash, breakup, re-entrainment, two-way coupling between continuous (air) and dispersed (water) phases and all four wheels spinning. The two-way particle-air coupling and wheel rotation were proved to be an important consideration to represent the correct physics, as demonstrated by Gaylard et at [11]. The one-way coupling does not enables the momentum transfer between the two phases, while the two-way coupling does.

A splash model was considered when liquid particles hit a surface, where these particles created child particles. The breakup model estimates when the aerodynamic shear causes a critical internal vibration to make a droplet to break-up and then splits the particle into child particles. The re-entrainment model calculated when the particle releases from a surface film: it allowed liquid to move along a surface, pool and re-enter the airflow as larger droplets. Jilesen

et al. [7] describes each model in greater detail. The liquid density was (ρ) 1000 kg/m3; dynamic viscosity was (μ) 1×10−3 Pa.s, and surface tension was (γ) 72.8×10-3 N/m.

For the self-soiling simulation, two tire emitters at the angle of 29.5 degrees and 326 degrees (Figure 7) were configured for each tire. The nozzles are located at the center of the tires and uniformly distributed particles at a 5deg cone half-angle. A standard deviation of 5 m/s was added and dripped particles larger than 0.3mm were re-entrained into the airflow. This simulation setup was based on PowerFLOW best practice and verified by Jilesen et at. [7]. The setup also included the vehicle speed at 100 km/h, water flow rate of 3.8 L/min and particle diameter of 0.165mm [5] (represents 1mm of water film on the road).

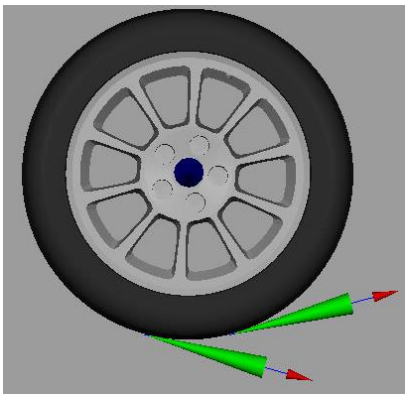

Figure 7. A schematic of tire emitter for self-soiling

For the rain setup, water is emitted from a plane in front of the car as shown in Figure 8. The particle diameter distribution is uniform, size of 2.05mm and emission rate of 17 mm/hr. According to Wikipedia.org/wiki/Rain [12] and USGS website [13], heavy rain precipitation rate is in between 10mm to 50mm per hour and raindrops have sizes ranging from 0.1 to 9 mm mean diameter but develop a tendency to break up at larger sizes.

Both load cases ran for 5s of simulation time and the results plotted in the paper were the last time step of each simulation in order to be comparable.

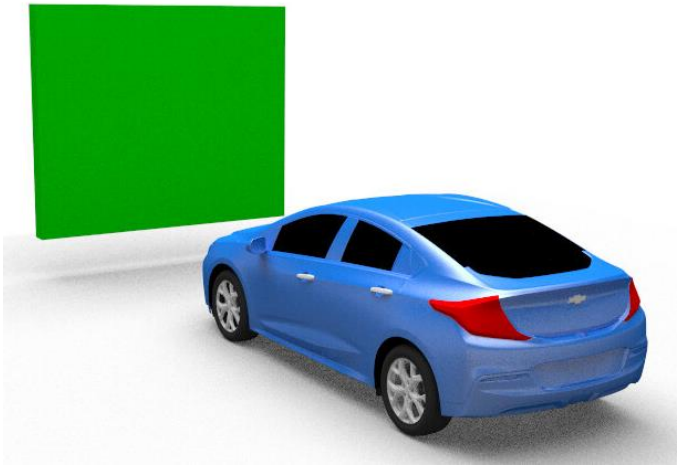

Figure 8. A schematic of plane emitter for rain

Results

The 2005 and 2004 models with and without the roof spoiler were simulated (Figure 9 and Figure 10 respectively).

Figure 9. 2005 Model with roof spoiler and with rear wiper

Figure 10. 2004 Model without roof spoiler and without rear wiper

Before running the contamination simulations, the regular aero simulation was performed at 110km/h to identify the aerodynamics behavior of those vehicles (Figure 11, 12, 13, 14). In Figure 11 (vehicle with the roof spoiler), in the velocity slice at the center of the model, it is possible to observe a clean flow separation happening at the spoiler trailing edge, creating a big aerodynamic wake. In addition, in Figure 12, where the velocity slice is moved closer to the C-Pillar, the flow separation is kept all the way to the corners.

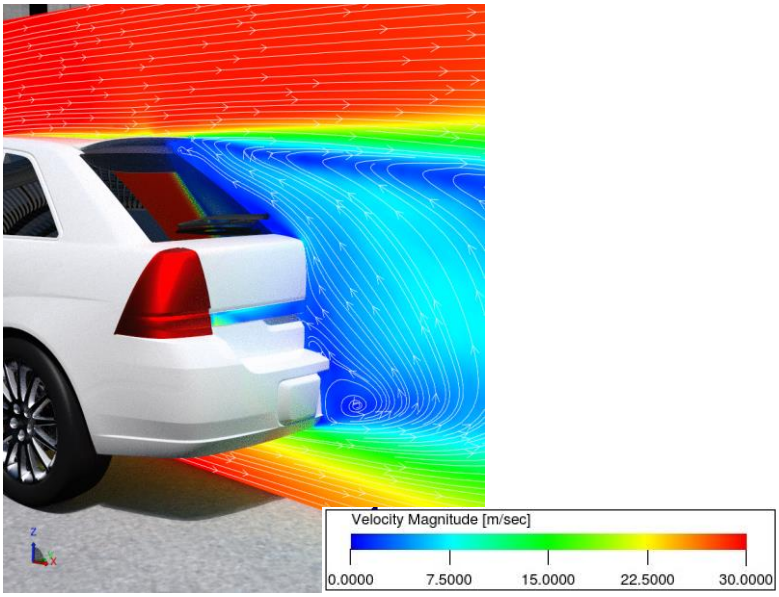

Figure 12. 2005 Model with roof spoiler: aero simulation showing air slice colored by velocity at centerline Y=0m

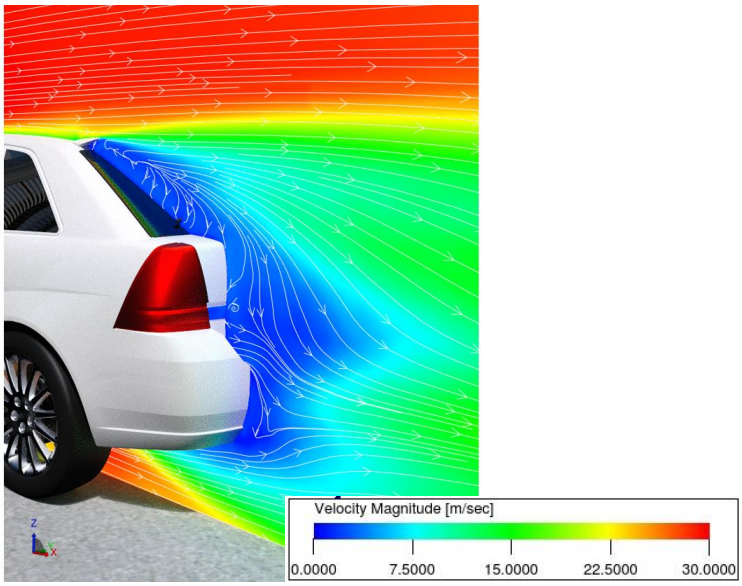

Figure 12. 2005 Model with roof spoiler: aero simulation showing air slice colored by velocity at Y=-0.5m

In Figure 12 (vehicle without roof spoiler), it is possible to observe in the velocity slice at the center of the model, the flow separation happening around the roof trailing edge, which generates a small air recirculation zone. However, in Figure 14, where the velocity slice is moved closer to the corner, the air flow presents higher velocity due to the wraparound caused by the C-Pillar vortex.

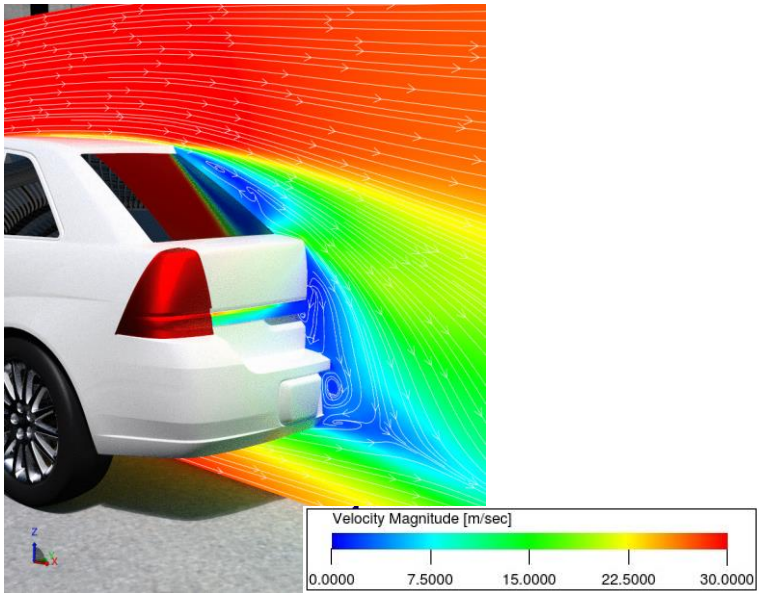

Figure 13. 2004 Model without roof spoiler: aero simulation showing air slice colored by velocity at centerline Y=0m

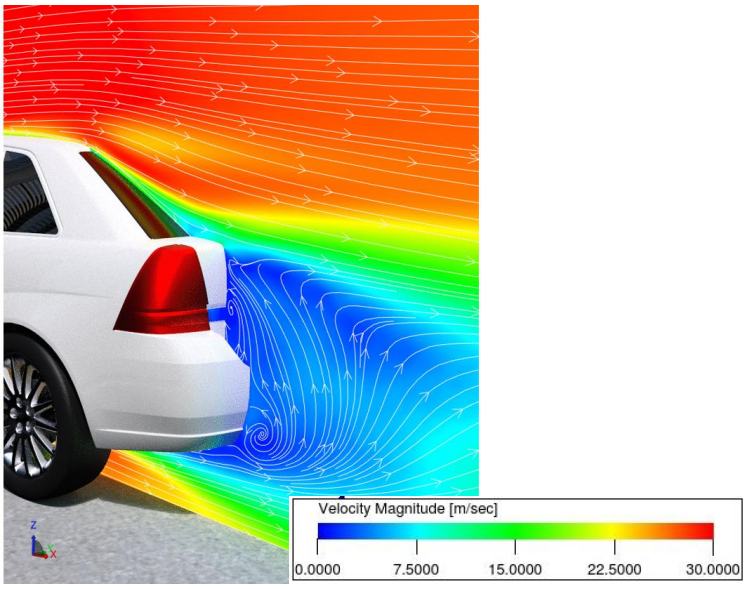

Figure 14. 2004 Model without roof spoiler: aero simulation showing air slice colored by velocity at Y=-0.5m

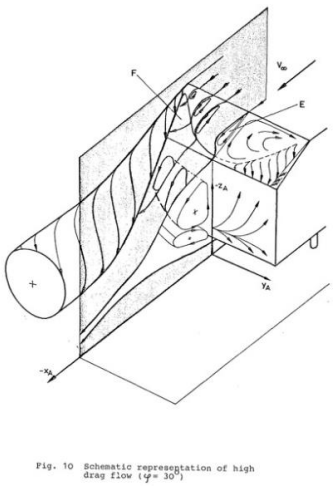

Fig. 10 Schematic representation of high drag flow ($\psi = 30°$)

Figure 15. Schematic representation of ξ = 30 degrees observed by Ahmed et al. [14]

The flow structure in Figures 13 to 14 is consistent with the expected flow structured observed by Ahmed et al [14] in Figure 15, where the absence of a roof spoiler generates a small recirculation zone at the center of the back glass and a higher velocity flow at the corners due to the C-Pillar vortex.

Once the rear aerodynamics behavior is comprehended (spoiler presented a greater aerodynamic wake once it separates the airflow from the vehicle surface), the contamination cases were performed (self-soiling and rain) according to the Simulation Setup section. Self-soiling results can be seen in Figure 16 and Figure 17, respectively with and without the roof spoiler. The results show the film thickness created by the contamination case.

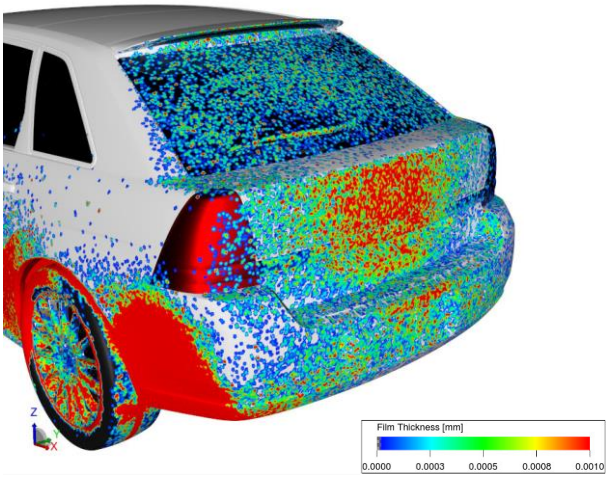

Figure 16. 2005 Model with roof spoiler: self-soiling results

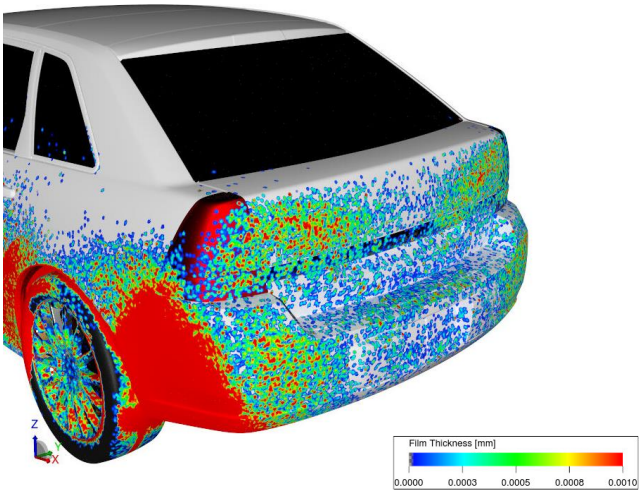

Figure 17. 2004 Model without roof spoiler: self-soiling results

The rain case was also evaluated in the numerical simulations and the results can be seen in Figure 18 and Figure 19, respectively with and without the roof spoiler. The results show the film thickness created by the rain case.

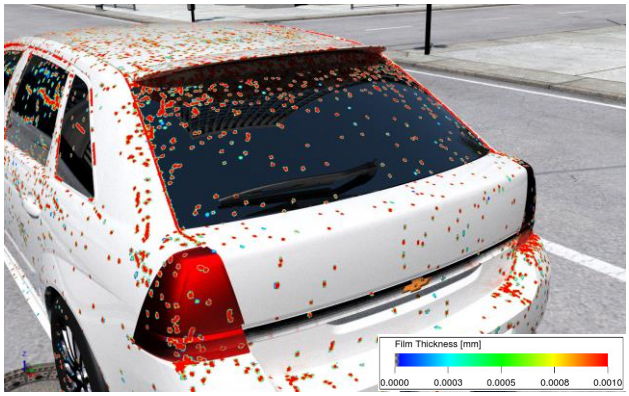

Figure 18. 2005 Model with roof spoiler: rain results

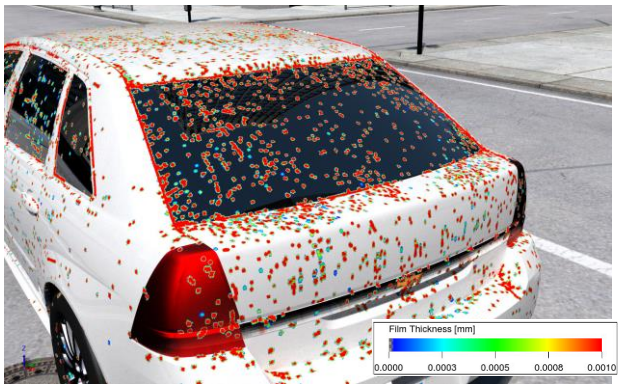

Figure 19. 2004 Model without roof spoiler: rain results

In order to objectively measure the back glass contamination, it was used the Contamination Index: is a measurement of the numbers of particles greater than 1x10-6m on a determined surface, i.e, density. For example, if 25% of the interested area is cover by film thickness larger than 1x10-6m, the contamination index is 25%.

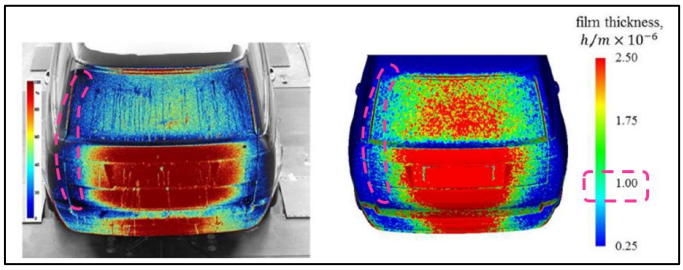

Figure 20. Comparison between physical test (left) and simulation (right) by Gaylard et al. [11]. It showed the smallest film thickness observed in the test was 1x10-6m

The self-soiling results for the 2005 model with spoiler presented a great number of particles on the back glass. That result was expected due to the flow separation starting at the trailing edge of the spoiler all the way until the corners. This car behaves as a squared back from an aerodynamics standpoint, where the particles on the ground are picked up by the tire motion, injected into the low pressure zone. If the back glass surface is inside the aerodynamic wake, those particles can be advected upwards to the back glass and attach to the glass surface, where there is a relatively higher base pressure. Such effect is described by Jilesen et al. [15] and can be observed in Figure 21.

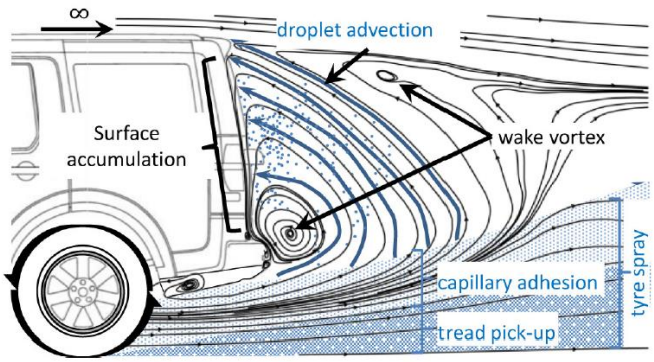

Figure 21. A schematic of rear surface contamination mechanisms on square back vehicles [16]

The 2004 model self-soiling results presented the backglass completely clean. That effect can be understood also by studying the aerodynamic wake. The upper bubble and attached flow are fed from the flow over the roof, which does not have contaminants into it. The upper flow structure is separated from the bottom one, where contaminants are present; hence, they cannot be advected up to the back glass. The 2005 model (with the roof spoiler) presented the contamination index of 14% after the 5 seconds of simulation time. While the 2004 model (without the roof spoiler) presented the contamination index of 0% during the same amount of time. The Contamination Index versus simulation time results were plotted in the Figure 22.

The same investigation was done for the rain cases. That one presented the opposite results observed on the self-soiling cases: 2005 model with roof spoiler presented less particles on the back glass compared with the 2004 model without roof spoiler. The Contamination Index was 7% for the model with the roof spoiler and 15% for the model without the roof spoiler. That means the spoiler is acting as an umbrella, protecting the back glass from the rain droplets. For the same aerodynamics reasons explained before, the flow over the backglass in the model without spoiler comes from the roof, which is carrying the rain droplets with it. Those droplets are constantly in contact with the back glass and running as rivulets.

Conclusions

Based on the Numerical Simulations, it is possible to conclude there is a significant difference in the flow field when the roof spoiler is included. That flow change also implies in different rear contamination results. Self-soiling loadcase showed film thickness on the back glass increased with the presence of the roof spoiler. However, the roof spoiler decreased the particles accumulation on the backglass in the rain loadcase. It was noted during durability tests

on dirty tracks at proving ground that the 2005 Malibu Maxx with the roof spoiler needed the rear wiper to keep the back glass clean to meet GM standards.

Based on the physical test information performed years ago (where the vehicle with the spoiler presented back glass contamination issues) and the simulation study presented in this paper (showing the spoiler increased the contamination for the self-soiling case only), it concludes the self-soiling load case is the worst case scenario for back glass contamination. That justify the manufacturer's decision to add the rear wiper for the commercial vehicle with the spoiler and proofs the current simulation tools available can predict rear end contamination very well.

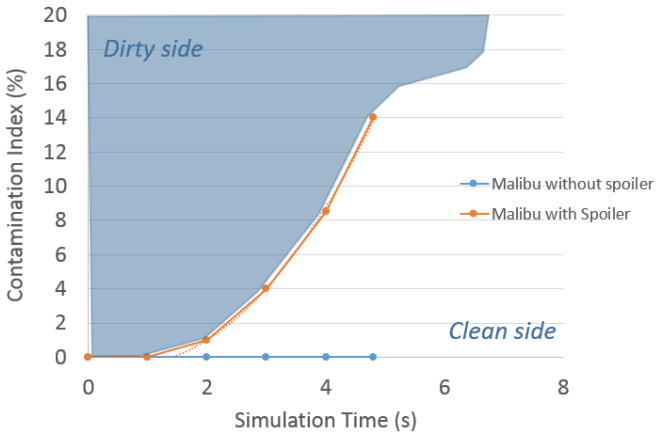

Figure 22. Self-soiling Contamination Index Plot versus Simulation Time

Another important data from this study was to set a threshold curve based on the Malibu Maxx study as reference for future vehicle development. If simulations for other vehicles present the Contamination Index above the threshold curve (blue area in Figure 22), it means the back glass contamination would be equal or worse than the model with roof spoiler and rear wiper would be required.

References

1. Gaylard, A., Kirwan, K., Lockerby D., "Surface contamination of cars: A review", in SAGE Journals, April 2017, doi:10.1177/0954407017695141.

2. Kuthada, T, Cyr, S. Approaches to vehicle soiling. In: 4th FKFS conference on progress in vehicle aerodynamics and thermal management: numerical methods (eds Wiedermann, J, Hucho, WH), Stuttgart, Germany, 2006, pp. 111–123. Renningen: Expert-Verlag.

3. Hagemeier, T., Hartmann, M., Thevenin, D., "Practice of vehicle soiling investigations: A review", International Journal of Multiphase Flow, 37 (2011) 860-875, www.elsevier.com/locate/ijmulflow

4. Goetz, H., "The Influence of Wind Tunnel Tests on Body Design, Ventilation, and Surface Deposits of Sedans and Sport Cars," SAE Technical Paper 710212, 1971, https://doi.org/10.4271/710212.

5. Jilesen, J., Alajbegovic, A., Duncan, B., “Soiling and Rain Simulation for Ground Transportation Vehicles”, 7th European-Japanese Two-Phase Flow Group Meeting, 2015, Zermatt, Switzerland.

6. Linfield, Kevin W., Mudry, Robert G., “Pros and Cons of CFD and Physical Flow Modeling”, Airflow Science Corporation, 2008. http://www.airflowsciences.com/.

7. Jilesen, J., Gaylard, A., Duncan, B., Konstantinov, A. et al., "Simulation of Rear and Body Side Vehicle Soiling by Road Sprays Using Transient Particle Tracking," SAE Int. J. Passeng. Cars - Mech. Syst. 6(1):2013, doi: 10.4271/2013-01-1256.

8. Mondo, C., Sommerfeld, M., Tropea, C. (1995). Droplet-wall collisions: Experimental studies of the deformation and breakup process in Int. J. Multiphase Flow, Vol 21, pp. 151-173.

9. O'Rourke, P.J., Amsden, A. A. (2000). A spray/wall interaction submodel for Kiva-3 wall film model in SAE Paper Nr. 2000-01-0271.

10. O'Rourke, P.J., Amsden, A. A. (1987). The TAB method for numerical calculations of spray droplet breakup in International Fuels and Lubricants Meeting and Exposition, Toronto.

11. Gaylard, A., Pitman, J., Jilesen, J., Gagliardi, A. et al., "Insights into Rear Surface Contamination Using Simulation of Road Spray and Aerodynamics," SAE Int. J. Passeng. Cars - Mech. Syst. 7(2):2014, doi:10.4271/2014-01-0610.

12. Wikipedia contributors, "Rain," Wikipedia, The Free Encyclopedia, https://en.wikipedia.org/w/index.php?title=Rain&oldid=929930494 (accessed January 25, 2020).

13. USGS – Science for a changing world (2019). https://water.usgs.gov/edu/activity-howmuchrain-metric.html (accessed January 25, 2020).

14. Ahmed, S., Ramm, G., and Faltin, G., "Some Salient Features Of The Time-Averaged Ground Vehicle Wake," SAE Technical Paper 840300, 1984, https://doi.org/10.4271/840300.

15. Jilesen, J., Gaylard, A., and Escobar, J., "Numerical Investigation of Features Affecting Rear and Side Body Soiling," SAE Int. J. Passeng. Cars - Mech. Syst. 10(1):2017, doi:10.4271/2017-01-1543.

16. Gaylard, A. P. (2016, 30 Nov.) "rear_soiling_mechanism.emf," https://dx.doi.org/10.6084/m9.figshare.4270085.v1 with an access on Dec 2019.

Contact Information

Aerodynamics CFD Engineer at General Motors: danilo.oliveira@gm.com

Acknowledgments

The authors would like to thank General Motors for permission to publish this paper and especially some people who supported this work:

Marcelo Bertocchi – GM CAE Director

Silvia Karlsson – GM Aerodynamics CFD Group Manager

Gena Vitale – GM Aerodynamics CFD Group Manager

Jacques Ndione – GM Aerodynamics CFD Engineer

Ben Ekola – GM Washer and Rear Wiper System Engineer

Bradley Gerwatowski – GM Wipers System Architect Engineer

Michael Demeo - Dassault System

Jeremy Beedy - Dassault System

Jonathan Jilesen - Dassault System

Definitions/Abbreviations

CFD Computational Fluid Dynamics

GM General Motors

6 ARTIGO 3: STUDY OF THE REAR BACKLIGHT ANGLE INFLUENCE ON VEHICLE AERODYNAMICS AND CONTAMINATION

Abstract

This paper examines the effect of rear effective backlight angle on vehicle contamination using contamination simulation results of a commercial vehicle. Highly-resolved time accurate computational fluid dynamics simulations were performed using a commercial Lattice-Boltzmann solver, to compare the rear end contamination with five different rear effective backlight angles. Additional aerodynamics simulations presented good correlation with published experimental data. The contamination results were compared with the aerodynamics simulation results in order to find trends between the two simulation types for different effective backlight angles.

Introduction

When analyzing contamination, the auto industry is mainly concerned with drivers' vision [1]. Gaylard et al. [2] describe contaminant as "any substance foreign to a particular vehicle surface and degrades the vision of drivers, the visibility of vehicles, system performance or aesthetic appeal". Under rain conditions, water accumulates on the windshield and back glass, often pulled out of the driver's view by wipers. The front wipers pushes the windshield water to and over the A-pillar to the side glass, causing driver visibility issues with the outside rear view mirrors. Other contamination issues on road vehicles include brake performance degradation and surface soiling, especially when driving on dirty, snowy or muddy roads. The three main contamination sources, according to Kuthada et al. [3] are: primary-contamination (wind-driven rain), foreign-contamination (from car ahead) and self-soiling (mist and dirt particles from the tire kick up, Figure 1). This paper solely focuses on the self-soiling load case (Figure 2).

Figure 1. Self-soiling phenomenon

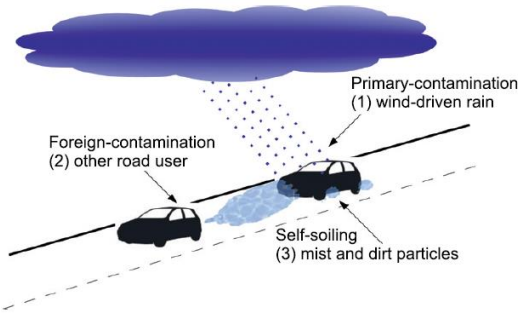

Figure 2. Three different origins for vehicle contamination: rain, foreign contamination and self-soiling [3]

To mitigate back glass contamination, car manufactures typically use rear wipers or air deflector. An example of an air deflector can be observed in Figure 3 (2004 Chevrolet Tahoe) as a back glass contamination countermeasure, but which can increase aerodynamic drag by around 20%, directly increasing fuel consumption [4].

Figure 3. 2004 Chevrolet Tahoe with air deflector to reduce back glass contamination

The effective backlight angle (ξ) described by Sims-Williams [5], also known as declination or slant angle, is the design variable studied in this paper. It defers from the backlight angle in cases where trunk, decklid or spoilers are present. The effective backlight angle is commonly defined as the angle that a line tangent to both the roof (point B in Figure 4) and rear compartment lid trailing edges (point A in Figure 4) at the vehicle centerline makes with a horizontal line, where the backlight angle is measured using the dashed line from Figure 4 instead. The effective backlight angle influences the aerodynamic drag being one of the parameters that dictates the location of the flow separation. Hucho et al. [6] showed how aerodynamic drag changes with the effective backlight angle (Figure 5). On vehicles with a steep effective backlight angle (e.g., station wagons with $\xi > 35$ degrees), the point of separation is at the rear edge of the roof. If ξ is reduced, at a given value, the separation line moves downwards from the rear edge of the inclined rear panel, which increases drag by 10%. The higher drag is attributable to strong trailing vortices with a corresponding rise in lift (Figure 5).

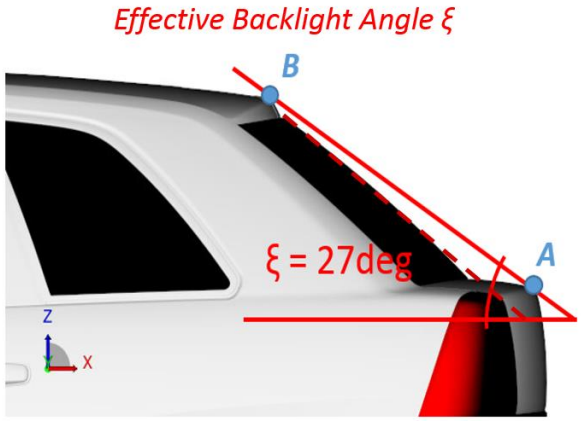

Figure 4. Effective backlight angle ξ

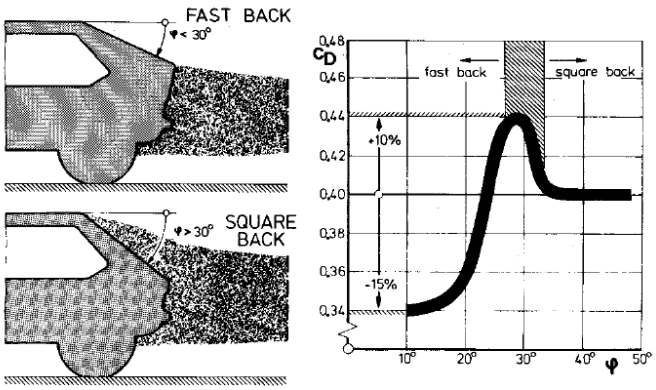

Figure 5. Coefficient of Drag versus Effective backlight angle ξ Plot [6]

The transition from square to fastback configurations exhibits distinct separation behaviors with relatively low drag. As observed by Hucho et al. [6], “it does not take place suddenly at a specific inclination angle limit, but in a transitional zone shown as a shaded area on the graph. In this transitional zone, the separation line oscillates between” the roof and the rear compartment lid in this case. If the angle is still further reduced, the drag again drops. At a fastback effective backlight angle of $\xi = 23$ degrees, the same reduced CD is obtained as the squareback flow pattern. To achieve lower drag angles, decklid spoilers are often implemented on sedans-type of cars, to reduce the effective backlight angle and consequently, reducing aerodynamic drag.

Usually for fastback vehicles, top left picture in Figure 5, for example, it is not often observed the presence of rear wiper. However, in squareback and SUV type of vehicles, bottom left picture in Figure 5 for example, contamination is usually observed on the back glass, warrants the need of rear wiper. Kabanovs et al. [7] published a similar contamination study with three different effective backlight angles on a generic SUV body using CFD and physical tests.

The motivation of the paper is to identify and analyze the relationship between aerodynamic drag and back glass contamination with respect to effective backlight angle.

Numerical Simulation

Aerodynamics Simulation

Compared to traditional wind tunnel tests, numerical simulations present quicker turnaround time, are cheaper to produce and enables in-depth investigations through the ability to plot and visualize multiple quantities on the vehicle surface. The Lattice-Boltzmann Method, implemented in the commercial software PowerFLOW, was used for the simulations presented in this paper. Jilesen et al. [8] describes the LBM method as the following: it is an inherently unsteady Lattice Boltzmann (LB) solver which uses what is essentially a Very Large Eddy Simulation (VLES) turbulence model.

The aerodynamic simulation setup used here followed lattice resolution and boundary conditions published in the PowerFLOW best practices for this type of vehicles (PowerFLOW user’s manual). It considered air velocity of 100 km/h and moving ground. In that regular aerodynamic simulation, all four wheels were spinning and the walls were 45m from the vehicle, which can be considered as an open domain (no influence of the side and top walls).

The lattice refinement was defined as shown in Figure 6. The coarsest element size on the top of the Figure 6 was 50mm and the finest element size closer to the vehicle surface was 2.5mm. The number of volumetric elements in each case was around 90 million.

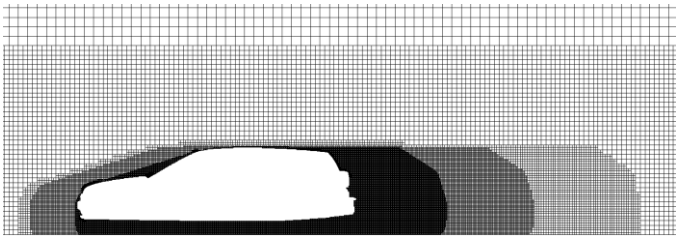

Figure 6. Volumetric Mesh Resolution

Contamination Simulation

In the past, contamination simulations were not well developed as it is nowadays, and vehicle development relied mainly on hardware tests. Currently, Computational Fluid Dynamics (CFD) tools can simulate fluid flow behavior for complex flows, including coupling particles and surface film models with time-accurate unsteady solutions [10]. Gaylard et al. [2], Jilesen et al. [8 and 9] and many other authors, performed comparison between this commercial software and physical tests in wind tunnel.

Once the Regular Aerodynamic simulation setup is completed, the Particle Modeling tool is turned on, which enables a film solver based on a Lagrangian particle simulator. The calculator assumes that particles form a thin film of fluid, which moves by the shear stresses. This simulator is formed by the splash model (studied by Mondo et al. [11] and O-Rourke and Amsden [12]), breakup model (specified by O-Rourke and Amsden [13]) and the re-entrainment model (which is defined by Jilesen et al. [8] as a critical film thickness of 0.3mm).

Gravity is also included and causes acceleration on the film of fluid, such as dripping. The resultant film momentum equation is:

$$\rho h \frac{D\vec{u}}{Dt} = -2\mu \frac{\vec{u}}{h} + \vec{\tau}_{air}(\vec{u}_*, \vec{n}) + \rho(\vec{g} - (\vec{g} \cdot \vec{n})\vec{n})h \quad (1)$$

where ρ is the density of the film, h is the film height, $\vec{u}$ is the film velocity, μ is the film viscosity, $\vec{n}$ is the surface normal, and $\vec{g}$ is the acceleration due to gravity. The shear stress resulting from the air moving over the film, τair, is dependent on the near wall air velocity, $\vec{u}*$, and is provided by the flow solver (Jilesen et al. [8]).

The two-way coupling enables the energy conservation for each particle. That is used to predict the trajectory of each particle, since they have their local drag force and momentum. The resultant reactionary force acting on the surrounding air is also considered. The equation for the particle acceleration is:

$$m\frac{D\vec{u}_{Particle}}{Dt} = \frac{1}{2}\rho C_D A(\vec{u}_{Particle} - \vec{u}_*)|\vec{u}_{Particle} - \vec{u}_*| + m\vec{g} \qquad (2)$$

where m is the particle mass, $\vec{u}$ is the particle velocity, CD is the drag coefficient for the particle, and A is the cross sectional area of the particle (Jilesen et al. [8]).

The coupling between the Lagrangian particle simulator with PowerFLOW allows millions of particles to be tracked simultaneously.

Simulation Setup

The CFD simulation used in this study included the particle splash, breakup, re-entrainment, two-way coupling between continuous (air) and dispersed (water) phases and all four wheels spinning. The two-way particle-air coupling and wheel rotation were proved to be an important consideration to represent the correct physics, as demonstrated by Gaylard et at [14]. The one-way coupling does not enables the momentum transfer between the two phases, while the two-way coupling does.

A splash model was considered when liquid particles hit a surface, where these particles created child particles. The breakup model estimates when the aerodynamic shear causes a critical internal vibration to make a droplet to break-up and then splits the particle into child particles. The re-entrainment model calculated when the particle releases from a surface film: it allowed liquid to move along a surface, pool and re-enter the airflow as larger droplets. Jilesen et al. [9] describes each model in greater detail. The liquid density was (ρ) 1000 kg/m3; dynamic viscosity was (μ) 1×10−3 Pa.s, and surface tension was (γ) 72.8×10-3 N/m.

For the self-soiling simulation, two tire emitters at the angle of 29.5 degrees and 326 degrees (Figure 7) were configured for each tire. The nozzles are located at the center of the tires and uniformly distributed particles at a 5deg cone half-angle. A standard deviation of 5 m/s was added and dripped particles larger than 0.3mm were re-entrained into the airflow. This simulation setup was based on PowerFLOW best practice and verified by Jilesen et at. [9]. The setup also included the vehicle speed at 100 km/h, water flow rate of 3.8 L/min and particle diameter of 0.165mm [8] (represents 1mm of water film on the road).

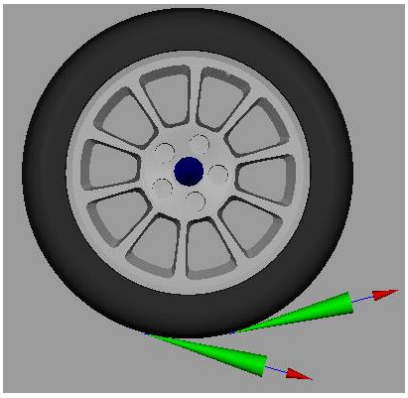

Figure 7. A schematic of tire emitter for self-soiling

The 2004 Malibu Maxx was selected as the baseline model for multiple reasons: it has an interesting effective backlight angle from the aerodynamic standpoint (ξ = 32 degrees), its rear end could be morphed from a fastback to a station wagon without distorting the vehicle shape and physical test results showed no reason for a rear wiper to be implemented. The model was simplified for simulation speed and cost, which included a flat underbody panel (no exhaust or fuel tank) and fully closed cooling grille openings (no flow to heat exchangers). Therefore, aerodynamic results from this study are not fully representative of the actual vehicle.

Initially, five different effective backlight angles were simulated using morphing tools. ξ = 21 degrees, ξ = 27 degrees, ξ = 32 degrees, ξ = 34 degrees and ξ = 45 degrees were considered and examples of the rear end shape can be observed in Figures 8, 9 and 10.

Figure 8. Rear end morphed to ξ = 21 degrees

Figure 9. Rear end morphed ξ = 32 degrees

Figure 10. Rear end morphed to ξ = 45 degrees

Results

Before running the self-soiling simulations, the aerodynamics simulation was performed to understand the flow behavior (Figures 11, 12, 13, 14 and 15).

The coefficient of drag obtained from the aerodynamics simulations is consistent with the trend observed by Hucho et al [6], in Figure 16. For an effective backlight angle of 21 degrees, the zero total pressure iso-surface, Figure 11, (CPT=0, used to visualize regions of separation) shows the air flow to be slightly separated at the center line of the roof trailing edge and C-pillars, but reattached for most of the back glass. The small wake along the back glass is isolated from the bigger wake that spans from the trailing edge of the decklid to the bottom of the rear fascia along with the rear wheelhouse. As the effective backlight angle increased, the upper wake around the backglass also grows, as seen in Figure 12 and Figure 13. For effective backlight angle of 34 degrees, the upper wake reaches a critical size where it begins to connect with the lower wake, as seen in Figure 14. When the angle is 45 degrees, Figure 15, the upper wake and lower wake integrate into one single larger wake. The observed drag behavior implies that an upper wake increases along with C-pillar vortices as the backlight angle increases. As the vortices become stronger due to the lower pressure on the surfaces they sit over, CD

increases up to the critical angle where the upper and lower wakes merge into one and drag drops. After that angle, backlight angle is not as sensitive. The flow structure in Figures 11 to 15 is consistent with the expected flow structured observed by Ahmed et al [15] in Figure 16.

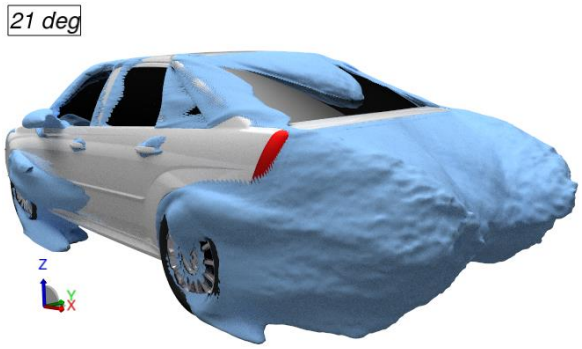

Figure 11. Iso Surface CPT=0 and rear end morphed to ξ = 21 degrees

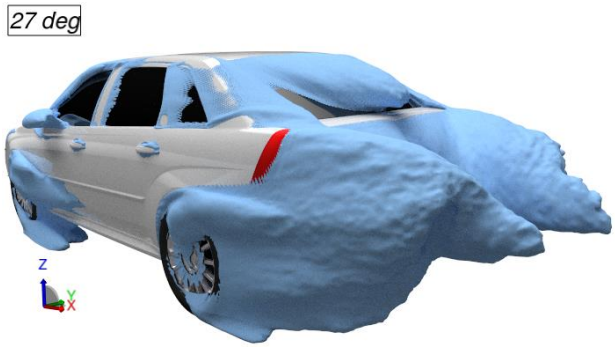

Figure 12. Iso Surface CPT=0 and rear end morphed to ξ = 27 degrees

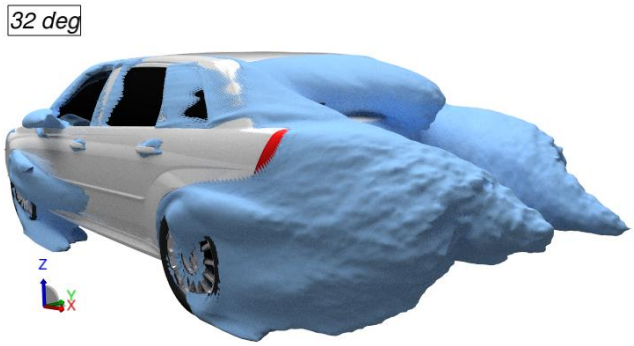

Figure 13. Iso Surface CPT=0 and rear end morphed to ξ = 32 degrees

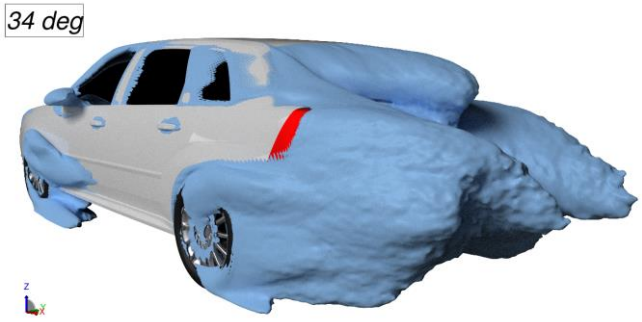

Figure 14. Iso Surface CPT=0 and rear end morphed to ξ = 34 degrees

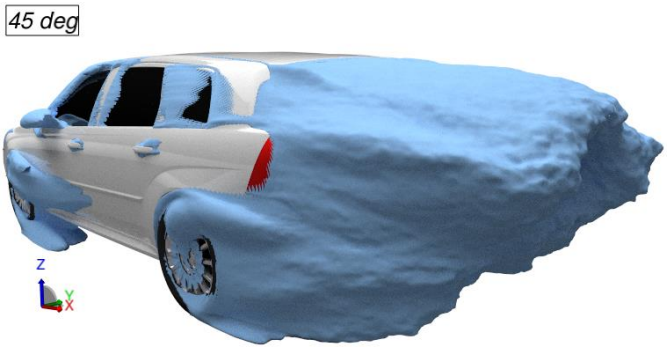

Figure 15. Iso Surface CPT=0 and rear end morphed to ξ = 45 degrees

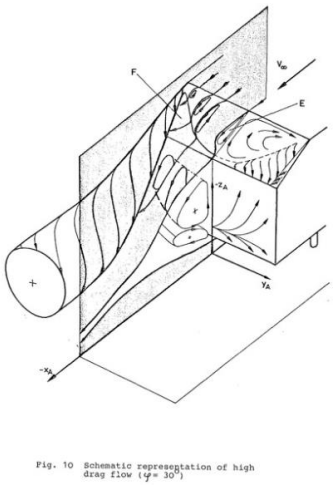

Fig. 10 Schematic representation of high drag flow ($\psi = 30°$)

Figure 16. Schematic representation of ξ = 30 degrees observed by Ahmed et al. [15]

The plotted CD behavior at different effective backlight angles exhibited a similar trend as seen by Hucho (Figure 6). ξ = 34 deg (Figure 14) case was simulated to better resolve the peak of the graph. The CD for that run was consistent with the rest of the curve (Figure 17). Simulation data is shown as closed circles were scaled by a constant in order the simulation data to match the experimental data at ξ = 20 deg (0.360 CD). These compare well to the measurements repored by Hucho et al [6] (solid line in black) except for ξ = 45 deg. That point

can be attributed due to a different vehicle geometries studied between simulation and test, specially at the C-pillar area. Also, it is not known the CFD bahaivor between ξ = 34 deg and ξ = 45 deg.

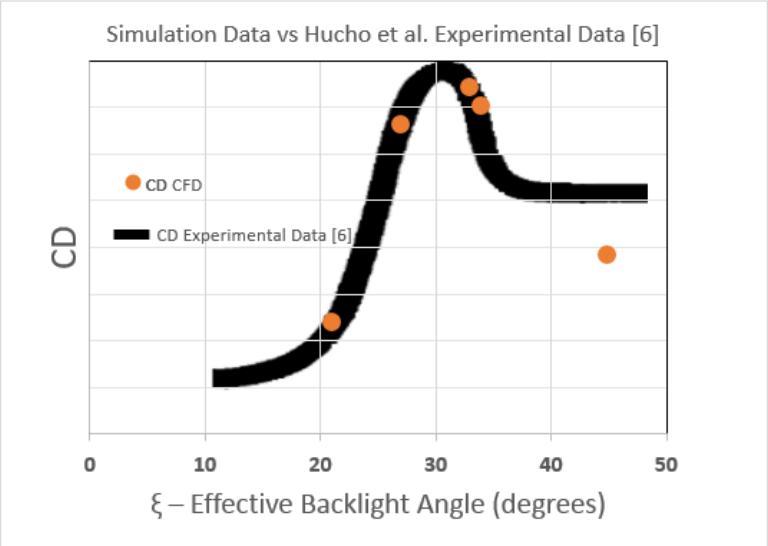

Figure 17. Coefficient of Drag versus Effective backlight angle ξ Plot

Following the aerodynamics simulation, the self-soiling simulations were performed. Water film thickness contours were plotted on the vehicle surface for the five simulated effective backlight angles, including ξ = 34 degrees (Figure 18, 19, 20, 21 and 22).

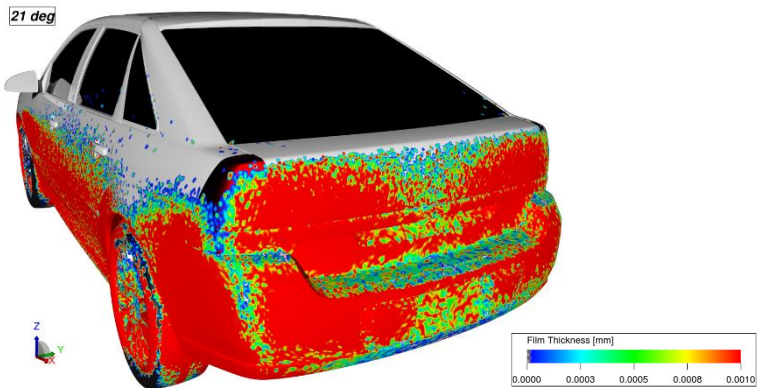

Figure 18. Film Thickness contour on rear end morphed to ξ = 21 degrees

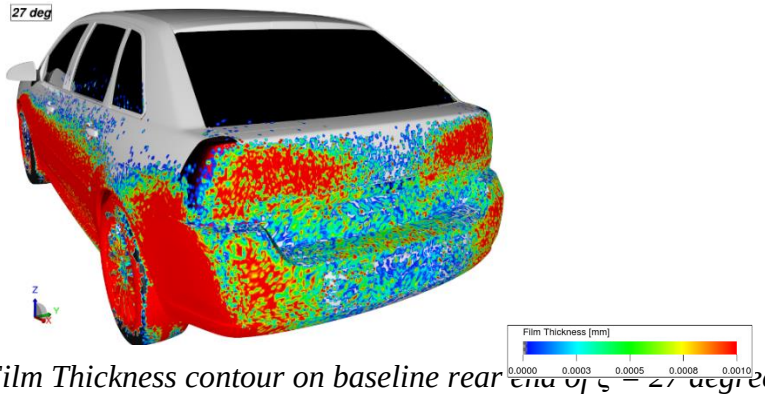

Figure 19. Film Thickness contour on baseline rear end of ξ = 27 degrees

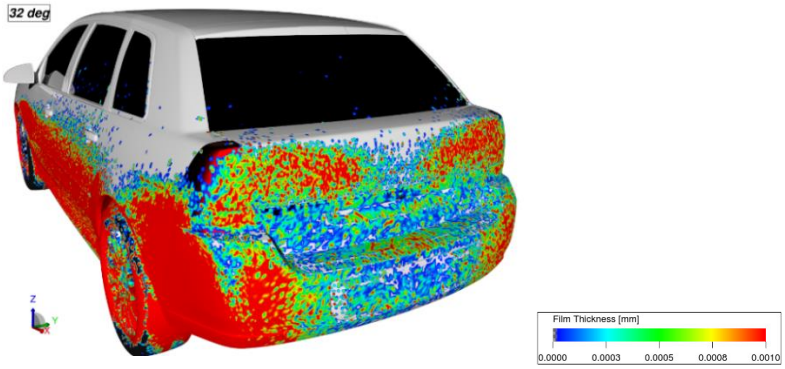

Figure 20. Film Thickness contour on rear end morphed to ξ = 32 degrees

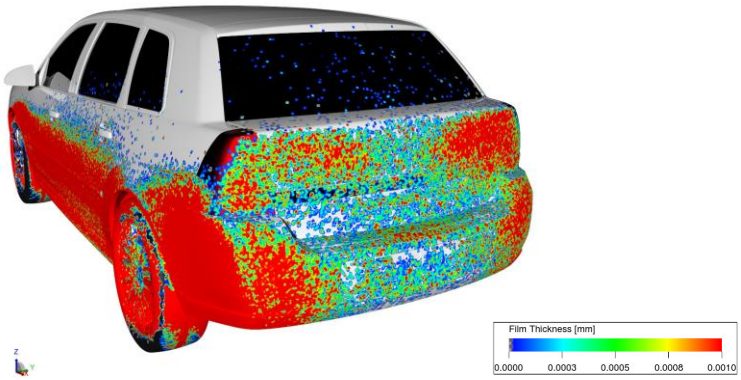

Figure 21. Film Thickness contour on baseline rear end of ξ = 34 degrees

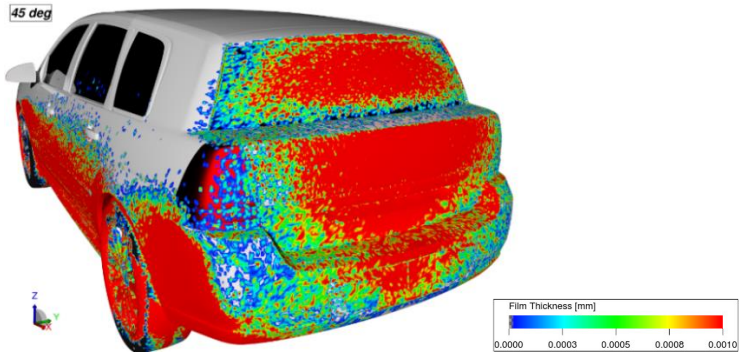

Figure 22. Film Thickness contour on rear end morphed to ξ = 45 degrees

The self-soiling simulation did not exhibit the same behavior as aerodynamic drag. Whereas drag peaks at a specific effective backlight angle of around ξ = 32 degrees, a direct relationship between film thickness and effective backlight angle was observed. As the effective backlight angle grows, the contamination on the back glass increases as well.

Self-soiling behavior can also be predicted by the rear wake topology. As also described by Gaylard et al. [2] "The physical reasons for this have become clear; droplets mainly thrown off the rear tires are carried into the wheel wakes from where they are transferred into the base wake, advected back towards the rear surfaces and deposited on them. Accumulation is most acute where the surface pressure is relatively high". For the squareback example in Figure 23 [17], the particles on the ground are picked up by the tire motion, injected into that low pressure zone. If the back glass surface is inside the aerodynamic wake, those particles can advect upwards to the back glass and attach to the glass surface. Such effect is described by Jilesen et al. [16].

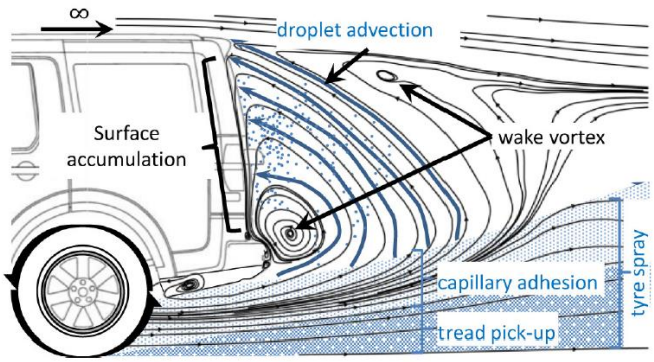

Figure 23. Schematic of rear surface contamination mechanisms on square back vehicles [17]

Per the simulation assumption (that simulates the contaminants being kicked up by the tires) contaminant are emitted on the tires surface, which are trapped inside the lower wake. In the lower effective backlight angles are studied (21, 27 and 32 degrees), where minimum particles accumulate on the back glass, the upper wake is still separate from the lower wake, where all the particles are trapped. At a 34 degrees effective backlight angle, the upper and the lower wakes begin to converge, creating a flow path for the particles inside the lower wake to navigate to the upper wake. Once the two wakes merges, a bigger intersection allows for bulk transport of contaminants from the lower wake zone into the upper wake zone, quickly increasing the film thickness of the back glass.

In order to objectively measure the back glass contamination, a Contamination Index was used which is defined as the number of particles greater than 1x10-6m on a determined surface (similar to a density). For example, if 25% of the interested area is cover by film thickness larger than 1x10-6m, the Contamination Index is 25%. The threshold of 1x10-6m was selected in the calculation of the contamination index based on the soiling coverage of the models simulated in this paper and corresponds with the data published in Gaylard et al. [2] (Figure 24).

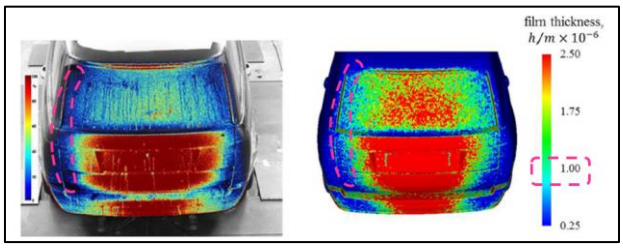

Figure 24. Comparison between physical test (left) and simulation (right) by Gaylard et al. [2].

Applying the Contamination Index measurement for the effective backlight angle cases (analyzing the backglass surface only), the Contamination Index for ξ = 21deg and 27 deg is 0%, for ξ = 32deg and 34deg is 1% and ξ = 45deg is 52%. Figure 25 shows the plot with CD and Contamination Index together versus the backlight angle. Where the backlight angle reaches the critical angle (peak of the experimental curve by Hucho et al. [6]), CD drops while back glass contamination increases.

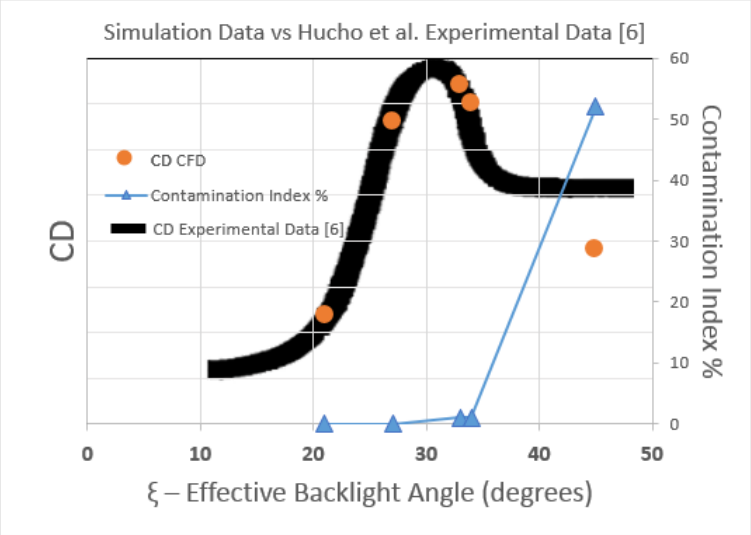

Figure 25. Coefficient of Drag and Contamination Index versus Effective backlight angle ξ Plot

The decklid is not the focus of this study, but it is shown in Figures 18 to 22 how the effective backlight angle also changes the contamination on the decklid rear face. The contamination on that area is affected by the wake topology as well: for ξ = 21deg, there is a weak downwash effect at the decklid trailing edge, keeping the base pressure relatively high and a very soiled area. As the effective backlight angle increases, the downwash wake becomes stronger, which makes the base pressure at the center of the rear face relatively lower, avoiding the contaminants deposition. When ξ = 45deg, the opposite happens (up wash) and the contaminants from the lower zone navigate to the upper zone, making the rear face of the decklid soiled.

Conclusions

Based on the results, it is possible to conclude that the effective backlight angle has a significant effect on the coefficient of drag as well as the back glass contamination. The influence of effective backlight angle on aerodynamic drag results correlates with the published experimental data studied by Hucho et al. [6]. A critical effective backlight angle, where the upper and lower wakes begin merging, associates aerodynamic drag behavior with back glass contamination together. At that critical angle, CD reaches a peak and starts to decrease (effective backlight angle around 34 degrees), as contaminants from the lower wake can now navigate to the upper wake and increasing the film thickness on the back glass.

This study only investigates the influence of the effective backlight angle, but other geometric changes on the rear end can also affect back glass contamination, such as the rear over hang, diffuser angle, roof spoilers shapes, etc. Those and a deep investigation in backlight angle between 34deg and 45deg for commercial vehicles are suggestions for future work in this area.

References

1. Hagemeier, T., Hartmann, M., Thevenin, D., “Practice of vehicle soiling investigations: A review”, International Journal of Multiphase Flow, 37 (2011) 860-875, www.elsevier.com/locate/ijmulflow

2. Gaylard, A., Kirwan, K., Lockerby D., “Surface contamination of cars: A review”, in SAGE Journals, April 2017, doi:10.1177/0954407017695141.

3. Kuthada, T, Cyr, S. Approaches to vehicle soiling. In: 4th FKFS conference on progress in vehicle aerodynamics and thermal management: numerical methods (eds Wiedermann, J, Hucho, WH), Stuttgart, Germany, 2006, pp. 111–123. Renningen: Expert-Verlag.

4. Goetz, H., "The Influence of Wind Tunnel Tests on Body Design, Ventilation, and Surface Deposits of Sedans and Sport Cars," SAE Technical Paper 710212, 1971, https://doi.org/10.4271/710212.

5. Sims-Williams, D., Marwood, D., and Sprot, A., "Links between Notchback Geometry, Aerodynamic Drag, Flow Asymmetry and Unsteady Wake Structure," SAE Int. J. Passeng. Cars – Mech. Syst. 4(1):156-165, 2011, https://doi.org/10.4271/2011-01-0166.

6. Hucho, W. H., Janssen, L. J., Emmelmann, H. J., "The Optimization of Body Details – A Method for Reducing the Aerodynamic Drag of Road Vehicle ", in SAE Paper Nr. 760185.

7. Kabanovs, A., Hodgson, G., Garmory, A., Passmore, M., Gaylard, A., "A Parametric Study of Automotive Rear End Geometries on Rear Soiling", in SAE Int. 2017, doi:10.4271/2017-01-1511.

8. Jilesen, J., Alajbegovic, A., Duncan, B., "Soiling and Rain Simulation for Ground Transportation Vehicles", 7th European-Japanese Two-Phase Flow Group Meeting, 2015, Zermatt, Switzerland.

9. Jilesen, J., Gaylard, A., Duncan, B., Konstantinov, A. et al., "Simulation of Rear and Body Side Vehicle Soiling by Road Sprays Using Transient Particle Tracking," SAE Int. J. Passeng. Cars - Mech. Syst. 6(1):2013, doi: 10.4271/2013-01-1256.

10. Linfield, Kevin W., Mudry, Robert G., "Pros and Cons of CFD and Physical Flow Modeling", Airflow Science Corporation, 2008. http://www.airflowsciences.com/.

11. Mondo, C., Sommerfeld, M., Tropea, C. (1995). "Droplet-wall collisions: Experimental studies of the deformation and breakup process" in Int. J. Multiphase Flow, Vol 21, pp. 151-173.

12. O'Rourke, P.J., Amsden, A. A. (2000). A spray/wall interaction submodel for Kiva-3 wall film model in SAE Paper Nr. 2000-01-0271.

13. O'Rourke, P.J., Amsden, A. A. (1987). The TAB method for numerical calculations of spray droplet breakup in International Fuels and Lubricants Meeting and Exposition, Toronto.

14. Gaylard, A., Pitman, J., Jilesen, J., Gagliardi, A. et al., "Insights into Rear Surface Contamination Using Simulation of Road Spray and Aerodynamics," SAE Int. J. Passeng. Cars - Mech. Syst. 7(2):2014, doi:10.4271/2014-01-0610.

15. Ahmed, S., Ramm, G., and Faltin, G., "Some Salient Features Of The Time-Averaged Ground Vehicle Wake," SAE Technical Paper 840300, 1984, https://doi.org/10.4271/840300.

16. Jilesen, J., Gaylard, A., and Escobar, J., "Numerical Investigation of Features Affecting Rear and Side Body Soiling," SAE Int. J. Passeng. Cars - Mech. Syst. 10(1):2017, doi:10.4271/2017-01-1543.

17. Gaylard, A. P. (2016, 30 Nov.) "rear_soiling_mechanism.emf," https://dx.doi.org/10.6084/m9.figshare.4270085.v1 with an access on Dec 2019.

Contact Information

Aerodynamics CFD Engineer at General Motors: danilo.oliveira@gm.com

Acknowledgments

The authors would like to thank General Motors for permission to publish this paper and especially some people who supported this work:

Marcelo Bertocchi – GM CAE Director

Silvia Karlsson – GM Aerodynamics CFD Group Manager

Gena Vitale – GM Aerodynamics CFD Group Manager

Jacques Ndione – GM Aerodynamics CFD Engineer

Donnell Johnson – GM Aerodynamics Test Engineer

Danyang Fan – GM Aerodynamics CFD Engineer

Ben Ekola – GM Washer and Rear Wiper System Engineer

Bradley Gerwatowski – GM Wipers System Architect Engineer

Michael Demeo - Dassault System

Jeremy Beedy - Dassault System

Jonathan Jilesen - Dassault System

Definitions/Abbreviations

CFD Computational Fluid Dynamics

CPT Coefficient of Total Pressure

GM General Motors

CD Coefficient of Drag

7 DISCUSSÃO

Nesse estudo foram realizadas simulações numéricas tridimensional multifásicas utilizando o método *Lattice-Boltzmann*. Foram analisadas condições de contaminação de sujeira vinda pelo chão e por chuva para veículos comerciais tanto em simulação em CFD quanto em testes em escala real em um túnel de vento climático, localizado na General Motors em Warren, EUA. Os resultados de contaminação no vidro traseiro foram validados em ambas ferramentas. Algumas variáveis foram estudadas, tais como vazão de contaminantes, velocidade do veículo, posição dos emissores, bem como influência de spoiler e do ângulo de inclinação do vidro traseiro.

Foi possível concluir do primeiro artigo, que as ferramentas computacionais utilizadas foram capazes de prever o mesmo direcionamento do teste, promovendo credibilidade para futuros estudos. A comparação inicial foi realizada por meio de imagens da espessura do filme de água na simulação e por fotos sob luz fluorescente no túnel de vento. Ainda foi desenvolvida uma metodologia para comparar os resultados de teste e simulação quantitativamente. Essa metodologia consiste em um programa desenvolvido em *Matlab* que conta os *pixels* de um selecionada imagem e aplica um contraste entre as cores (foto torna-se bi-color). As duas cores de *pixels* são contabilizadas em uma determinada área e a razão entre esse número é a densidade de contaminação no vidro traseiro. Um método semelhante foi desenvolvido na análise numérica, chamado de Índice de Contaminação. Este método contabiliza partículas acima de 0.001mm de espessura de água em uma determinada área e calcula a porcentagem dessas partículas que cobre tal área. Esses métodos foram utilizados para comparar os resultado quantitativamente entre simulação e teste e entre simulações.

A fim de se verificar os parâmetros do modelo de simulação recomendados pelo fabricante do *software*, alguns estudos foram feitos. As resoluções de malha estudadas foram baseadas no recomendado pelo fabricante do *software*, na qual o menor elemento da malha volumétrica é de 2.5mm. Os resultados dobrando o tamanho dessa malha ou reduzindo pela metade, não mostraram significativa alteração no Índice de Contaminação no vidro traseiro (na ordem de 0.2%), mas visualmente, a malha mais grosseira apresenta mais partículas ao passo que a malha mais refinada mostrou resultados semelhantes ao modelo inicial. Contudo, o custo computacional da malha mais refinada foi praticamente o dobro no modelo inicial. Dessa forma, a recomendação do fabricante do *software* foi utilizado para futuras simulações.

A vazão de fluido pelos emissores nos pneus também foi estudada, e como visto anteriormente por Gaylard et al. (2017), o acúmulo de massa é linear com o tempo, o que significa que quanto maior a vazão de fluído, mais rapidamente se atinge um regime permanente, sugerindo pouco tempo de simulações numéricas podem ser comparadas a longos testes experimentais. Dessa forma, o valor inicial de vazão permaneceu para as futuras simulações.

Outro parâmetro estudado foi a velocidade do veículo: 50km/h e 100km/h. A conclusão é semelhante a do estudo da vazão de fluído, pois o aumento da velocidade implica em maior velocidade de rotação das rodas, que consequentemente, aumenta a vazão de fluido. Assim, a velocidade mais alta foi escolhida para as subsequentes simulações.

O último parâmetro não geométrico estudado na simulação de auto-contaminação foi o tamanho e distribuição das partículas. Jilesen et al. (2015) apresentaram um estudo usado como referência pelo fabricante do *software* no qual um determinado diâmetro de partículas (0.165mm) com distribuição uniforme é recomendado. Um outro estudo realizado por Strohbucker et al. (2019) mostra uma distribuição gaussiana com partículas de 0.2mm de diâmetro e desvio padrão 0.05mm. Os resultado na região do vidro traseiro são semelhantes para as duas propostas, e o método de Jilesen et al. foi adotado nesse trabalho.

Para as simulações de chuva, técnicas semelhantes ao da auto-contaminação foram utilizadas, com os emissores na frente do carro ao invés de estarem próximos à roda. O tamanho do domínio foi estudado, de forma em que foram simulados o domínio aberto e o domínio com as dimensões do túnel de vento da General Motors, e os resultados de contaminação do vidro traseiro não foi influenciado por esse fator. Maiores vazões de água possibilitaram a simulação atingir um regime permanente mais rapidamente (conclusão semelhante ao caso de auto-contaminação). O tamanho das partículas, contudo, influenciaram a contaminação no vidro traseiro, de forma que quanto maior o tamanho das partículas, maior o Índice de Contaminação no vidro traseiro. Uma outra variação foi a altura do tubo com os emissores de água em relação ao chão do túnel, o qual não afetou a distribuição das partículas no vidro traseiro, mas aumentou a espessura do filme de água conforme essa altura do tubo em relação ao chão aumenta. O ângulo de abertura dos emissores influenciaram os resultados de contaminação no vidro traseiro: quanto menor o ângulo, menor o Índice de Contaminação, mas a distribuição foi a mesma. Alterando o método de emissão de água dos três bico injetores para o plano na frente do modelo, observou-se maior acúmulo de água no vidro traseiro. O método utilizando o plano é o recomendado pelo fabricante do *software*, contudo uma reprodução mais semelhante ao túnel de vento com os três bicos injetores foi utilizada nas análise subsequentes. Em conclusão,

para qualquer estudo feito, o vidro traseiro sempre apresentava contaminação pela simulação numérica.

Com respeito aos resultados do túnel de vento, a auto-contaminação não apresentou nenhuma partícula de água independente da posição do emissor (na frente ou atrás da roda) e da velocidade do fluxo de ar (100km/h ou 50km/h). Esse resultado está de acordo com o previsto pelas simulações numéricas, nas quais o Índice de Contaminação no vidro traseiro foi de 0% para essa condição. As mesmas regiões da traseira do carro que apresentaram baixa espessura de filme de água na simulação, também apresentaram baixa contaminação no teste físico, como por exemplo na área abaixo da lanterna traseira. O oposto também foi observado, em regiões em que a espessura do filme de água é elevado na simulação, também apresentou alta contaminação no teste.

Na análise qualitativa comparando-se o teste com a simulação, uma ferramenta no *software Adobe Photoshop* foi utilizada, na qual a saturação na cor da mistura de água com contraste foi alterada, a fim de destacar as regiões com maiores concentrações da mistura. Assim, em regiões como a lanterna traseira, em que não se consegue observar partículas de mistura a princípio, utilizando essa técnica, foi possível verificar pequenas partículas, o que corrobora com os resultados da simulação (espessura do filme de 0.002mm). Na análise quantitativa, a metodologia pelo *Matlab* descrita anteriormente foi utilizada, e o resultado mostrou que, tanto na simulação quanto no teste, a contaminação no caso de auto-contaminação foi de 0%.

Os resultados de teste de chuva mostraram que independente da altura do tubo com os emissores em relação ao chão do túnel de vento, o vidro traseiro não apresentava nenhuma partícula de mistura, mesmo que o vídeo em tempo real do teste mostrava que havia uma grande quantidade de fluído ao redor da traseira do veículo. O principal motivo desse fenômeno é devido aos canais de drenagem e *gaps* entre os painéis externos do veículo. Esses impediam com que a mistura atingisse o vidro traseiro, uma vez que observou-se a mistura escorrendo por dentre esses espaço. Para verificar essa hipótese, fitas adesivas foram instaladas de forma que esses canais foram totalmente selados. Com essa última configuração, observou-se a mistura correndo pelo vidro traseiro, semelhantemente aos resultados da simulação numérica.

A metodologia pelo *Matlab* também foi utilizada para os testes de chuva. Quando comparados com a simulação, 11% do vidro traseiro apresentou partículas da mistura no teste e 7% para a simulação. Essa diferença pode ser explicada pelo fato dos fluídos serem diferentes (água pura na simulação e mistura de água com pó de contraste no teste), pela diferença entre rugosidade de materiais apresentada no carro real (metal, borracha e vidro), enquanto na

simulação todas as regiões apresentam rugosidade nula; e por fim, a fita adesiva utilizada para selar os canais de drenagem, possui uma certa espessura, a qual altera o fluxo da mistura vinda do teto do carro.

Contudo, apesar de algumas limitações no modelo de CFD, como por exemplo detalhes de canais de drenagem de água, os quais não foram representados na simulação e representam um importante papel para a condição de chuva, os resultados da simulação apresentaram boa correlação com o teste, de forma que podem ser utilizadas para prever contaminação no vidro traseiro devido a auto-contaminação ou chuva.

No tocante a contaminação do vidro traseiro, observou-se uma mudança substancial da esteira aerodinâmica quando um *spoiler* é adicionado ao teto do carro. Esse assunto se tornou material para o segundo artigo presente nesse trabalho. E baseado nos resultados e também em citações no artigo, notou-se que essa alteração na esteira aerodinâmica também altera a deposição de partículas de sujeira no vidro traseiro. Para o caso de auto-contaminação, a presença do *spoiler* aumentou a contaminação no vidro traseiro, enquanto para a condição de chuva, o *spoiler* reduziu a contaminação na mesma região. Baseado em dados da empresa montadora do carro estudado (quando o *spoiler* foi adicionado no modelo do ano seguinte, um limpador do vidro traseiro teve que ser implementado devido a contaminação no vidro traseiro vista em testes de durabilidade no campo de provas), conclui-se que o caso de auto-contaminação é o caso mais crítico para estudos de contaminação de vidro traseiros em veículos automotivos, uma vez que adicionando o *spoiler* aumentou-se a contaminação apenas no caso de auto-contaminação.

Um dos efeitos do *spoiler* é a mudança do ângulo de inclinação efetivo do vidro traseiro, que tem uma função da aparência do carro e também gera uma alteração aerodinâmica. Por esse motivo, o ângulo de inclinação do vidro traseiro foi o alvo de estudo do terceiro artigo apresentado nesse trabalho. Esse ângulo foi modificado a partir do modelo base em diversos valores e simulações aerodinâmicas e de contaminação foram estudadas.

Os valores do coeficiente de arrasto plotados contra o ângulo de inclinação apresentaram o mesmo formato da curva experimental gerada por Hucho et al. (1976), com exceção ao último ponto (45º). O motivo desse último ponto ter saído fora do estudo experimental citado, pode ser devido a diferenças geométricas externas entre os modelos (testado por Hucho et al. (1976) e o modelo numérico estudado), especialmente na região do *spoiler* no teto, da tampa do porta malhas e da coluna C. Foi observado também que há um valor crítico do ângulo de inclinação, em torno de 32º a 34º, no qual o coeficiente de arrasto muda drasticamente devido as esteiras superior e inferior se unificarem. Nessa condição, inicia-se uma deposição de contaminantes no

vidro traseiro, uma vez que a esteira inferior, onde há recirculação de contaminantes no ar, une-se com a esteira superior, até então, com ar limpo. Os resultados de coeficiente de arrasto e contaminação foram plotados num mesmo gráfico para visualizar o efeito e é notado que a partir do ângulo crítico (32º ~ 34º), o coeficiente de arrasto decresce enquanto o Índice de Contaminação cresce.

8 CONCLUSÕES

A conclusão geral desse trabalho foi que ferramentas numéricas de CFD, neste caso utilizando metodologia *Lattice-Boltzmann*, são capazes de prever a contaminação no vidro traseiro de veículos automotivos. Além disso, por meio de tais ferramentas, é possível compreender quais fatores influenciam na contaminação do vidro traseiro, o que permite definir, em novos projetos, se há necessidade de limpadores de vidro traseiro, baseando-se nos resultados numéricos. Por fim, ainda pode-se aliar os fatores que influenciam na contaminação do vidro traseiro com o coeficiente de arrasto aerodinâmico, a fim de otimizar essas duas disciplinas ao mesmo tempo.

Trabalhos Futuros

Devido a ausência de canais de drenagem de água no modelo de simulação, não foi possível encontrar uma boa comparação do caso de teste de chuva entre o túnel de vento e simulação. Uma sugestão de futuro trabalho seria aumentar a fidelidade do modelo de simulação, representando os canais de drenagem para comparar com os resultados do túnel de vento.

Outra sugestão é fazer estudo de contaminação em sensores e câmeras de veículos autônomos tentando otimizar o posicionamento das mesmas ou criar geometrias que evitam a contaminação das mesmas e também de estudar ângulos de inclinação do vidro traseiro intermediários entre 34º e 45º.

REFERÊNCIA GLOBAL

Hucho, W. H., Janssen, L. J., Emmelmann, H. J., “The Optimization of Body Details – A Method for Reducing the Aerodynamic Drag of Road Vehicle “, in SAE Paper Nr. 760185 (1976).

Schilling, F., Kuthada, T., Gaylard, A., Wiedemann, J. et al., “Advances in Experimental Vehicle Soiling Tests,” SAE Technical - Paper 2020-01-0681, 2020, doi:10.4271/2020-01-0681.

Strohbücker, V., Niesner, R., Schramm, D., Kuthada, T. et al., “Experimental Investigation of the Droplet Field of a Rotating Vehicle Tyre,” SAE Technical Paper 2019-01-5068, 2019, doi:10.4271/2019-01-5068.

Gaylard, A. P.; Kabanovs, A.; Jilesen, J.; Kirwan, K.; Lockerby, D.A.; “Simulation of rear surface contamination for a simple bluff body”, Journal of Wind Engineering and Industrial Aerodynamics, 2017.

Jilesen, J., Alajbegovic, A., Duncan, B., “Soiling and Rain Simulation for Ground Transportation Vehicles”, 7th European-Japanese Two-Phase Flow Group Meeting, 2015, Zermatt, Switzerland.